Progress in Aerospace Sciences 130 (2022) 100810

Contents lists available at ScienceDirect

Progress in Aerospace Sciences

journal homepage: www.elsevier.com/locate/paerosci

Non-intrusive flow diagnostics for unsteady inlet flow distortion measurements in novel aircraft architectures

Ulrich Doll [a,*], Matteo Migliorini [b], Joni Baikie [b], Pavlos K. Zachos [b], Ingo Röhle [c], Sergey Melnikov [c], Jonas Steinbock [d], Michael Dues [d], Ralf Kapulla [a], David G. MacManus [b], Nicholas J. Lawson [e]

[a] Experimental Thermal-Hydraulics Group, Paul Scherrer Institute, Forschungstrasse 111, Villigen PSI, 5232, Switzerland
[b] Propulsion Engineering Centre, Cranfield University, MK43 0AL, Cranfield, United Kingdom
[c] Berliner Hochschule für Technik, Luxemburger Str. 10, Berlin, 13353, Germany
[d] ILA R&D GmbH, Rudolf-Schulten-Straße 3, Jülich, 52428, Germany
[e] School of Aerospace, Mechanical & Mechatronic Engineering, The University of Sydney, Rm N304, J11 Level 3, Sydney, NSW 2006, Australia

ARTICLE INFO

Keywords:
Air induction systems
Convoluted diffusers
Inlet flow distortion
Unsteady flow
Propulsion integration
Non-intrusive flow diagnostics
Seeding-free measurements
Laser based flow measurements
Filtered Rayleigh Scattering (FRS)

ABSTRACT

Inlet flow distortion is expected to play a major role in future aircraft architectures where complex air induction systems are required to couple the engine with the airframe. The highly unsteady distortions generated by such intake systems can be detrimental to engine performance and were previously linked with loss of engine stability and potentially catastrophic consequences. During aircraft design, inlet flow distortion is typically evaluated at the aerodynamic interface plane, which is defined as a cross-flow plane located at a specific upstream distance from the engine fan. Industrial testing currently puts more emphasis on steady state distortions despite the fact that, historically, unsteady distortions were acknowledged as equally important. This was partially due to the limitations of intrusive measurement methods to deliver unsteady data of high spatial resolution in combination with their high cost and complexity. However, as the development of aircraft with fuselage-integrated engine concepts progresses, the combination of different types of flow distortions is expected to have a strong impact on the engine's stability margin. Therefore, the need for novel measurement methods able to meet the anticipated demand for more comprehensive flow information is now more critical than ever. In reviewing the capabilities of various non-intrusive methods for inlet distortion measurements, Filtered Rayleigh Scattering (FRS) is found to have the highest potential for synchronously characterising multiple types of inlet flow distortions, since the method has the proven ability to simultaneously measure velocity, static pressure and temperature fields in challenging experimental environments. The attributes of the FRS method are further analysed aiming to deliver a roadmap for its application on ground-based and in-flight measurement environments.

1. Introduction

Novel propulsion systems and their integration with the airframe are expected to play a key role in achieving aviation's long-term sustainability targets. International aviation strategic reports from EASA, NASA and ICAO call for a dramatic reduction in CO_2 and NO_x emissions [1–3]. Reaching these goals will require substantial developments to the airframe and the propulsion system, resulting in unconventional architectures such as boundary layer ingestion (BLI) and distributed propulsion. In these future designs, the engine face will be confronted with highly unsteady and distorted inflow characteristics.

Steady-state inlet flow distortion (i.e. variations in air pressure, temperature and angularity at the inlet plane of an aero-engine) and associated engine stability margins are relatively mastered on current aircraft designs with under-wing engine configurations. However, future commercial aircraft concepts are moving towards novel, closely coupled airframe-engine architectures with convoluted intakes to supply the propulsion system with the required mass flow. This presents a growing need to better understand the influence of unsteady inlet distortions on the stability of the engine across all phases of flight. Unsteady distortions generated by the intake were previously found to be detrimental to engine performance, but may also trigger rotor blade vibrations that can result in reduced component lifetimes or, in extreme cases, cause compressor surge or catastrophic damage to

* Corresponding author.
E-mail address: ulrich.doll@psi.ch (U. Doll).

https://doi.org/10.1016/j.paerosci.2022.100810
Received 8 October 2021; Received in revised form 10 February 2022; Accepted 19 February 2022
Available online 9 March 2022

Nomenclature

Acronyms

3C	Three-component
AIM	Advanced In-flight Measurement techniques
AIP	Aerodynamic Interface Plane
AIR	Aerospace Information Report
ARP	Aerospace Recommended Practice
BLI	Boundary Layer Ingestion
CRBS	Coherent Rayleigh–Brillouin Scattering
CRM	Common Research Model
CW	Continuous Wave
DGV	Doppler Global Velocimetry
FLEET	Femtosecond Laser Electronic Excitation Tagging
FRS	Filtered Rayleigh Scattering
FWHM	Full Width at Half Maximum
IR	Infrared
IRS	Interferometric Rayleigh Scattering
L2F	Laser-2-Focus
LDA	Laser Doppler Anemometry
LIDAR	Light Detection And Ranging
LIF	Laser Induced Fluorescence
MPR	Multiple Per Revolution
MTV	Molecular Tagging Velocimetry
NGV	Nozzle Guide Vane
NTF	National Transonic Facility
OPO	Optical Parametric Oscillator
PDV	Planar Doppler Velocimetry
RELIEF	Raman Excitation and Laser-Induced Electronic Fluorescence
S-PIV	Stereoscopic Particle Image Velocimetry
SAE	Society of Automotive Engineers
SD	Swirl Directivity
SI	Swirl Intensity
SNR	Signal-to-Noise-Ratio
SP	Swirl Pairs
SS	Sector Swirl
UV	Ultra violet
VTOL	Vertical Take-Off and Landing

Greek symbols

ρ	Density
θ	Critical sector angle

Roman symbols

ΔP	Total pressure variation
c	Concentration
P	Total pressure
p	Static pressure
P_{avg}	Average total pressure over full AIP
T	Temperature
v	Velocity

Subscripts

c	Circumferential
r	Radial

engine components. These assessments will be required throughout the aircraft's development phases as the design is matured, initially through numerical means, then ideally in ground test facilities followed by in-flight testing. To unlock the full potential of these novel concepts, a close integration of airframe, intake and engine design is imperative.

Current practice for aero-engine testing and safety certification relies on only a few intrusive measurements of pressure and temperature (at a low temporal and spatial resolution) to quantify the flow distortion levels at the engine face. Although unsteady flow distortion has been identified as a key detrimental factor to aero-engine stability, the low maturity of advanced flow measurement methods in combination with the high risk of integrating complex measurement systems into engine test facilities have prevented the development of design metrics for distortion tolerant aero-engines. Consequently, the necessity for richer instantaneous data to aid the understanding of the flow distortions that lead to engine stall events remains a key requirement. This becomes even more critical as industry is moving towards an era of strongly close-coupled engine-aircraft configurations. Given the known limitations of conventional methods (low spatial and temporal resolution, and intrusive instruments that interact with the flow), existing technologies are inadequate to sufficiently reduce the risk on the development of future systems.

To support this ongoing transformation process, the purpose of this review article is to provide a comprehensive overview on the topic of inlet flow distortion in the context of future airframe-integrated propulsion systems. After presenting a few examples of these novel concepts, the article provides an introduction to the phenomenology of inlet flow distortion, discusses the effects that inlet flow distortion can have on a propulsion system, how inlet flow distortion is described mathematically and current measurement practices of the pertinent flow quantities. The second part of the review initially describes the state-of-the-art in non-intrusive distortion measurement, points to drawbacks of current methods and formulates requirements that future measurement technology should be able to meet. This motivates a review of seeding-free laser-optical measurement techniques from the viewpoint of their potential for characterising complex technical flows, specifically with respect to the future ability to use these methods along the entire engine development cycle in ground and flight tests, which ultimately requires the use of optical probes. From the short list of available methods, the filtered Rayleigh scattering (FRS) technique is found to clearly have the highest potential to characterise inlet flow distortions in convoluted intake architectures. The article then continues with a description of current technological hurdles and concludes with an outlook on future FRS instrumentation as an enabler for advanced, seeding-free, optical flow measurements pertinent to in-situ ground and in-flight test scenarios.

2. Inlet flow distortion in novel propulsion systems

2.1. Overview of novel aero-engine architectures

Novel concepts for civil transport aircraft incorporate unconventional aero-engine propulsion system architectures (Figs. 1–3). Although the designs have overall benefits in terms of efficiency and noise [4], these architectures present more significant engine-airframe interaction effects compared to the conventional arrangement of engines on pylons under the wing [5,6]. At cruise conditions, conventional under-wing podded engines ingest relatively "clean", undisturbed airflow, while the unconventional designs embed the engine intakes in the fuselage, which leads to the inlet airflow ingested by the engines being highly distorted by the upstream airframe geometry. This has consequences for engine stability and efficiency [6,7].

Fig. 1. Artist's Impression of the CENTRELINE turbo-electric propulsive fuselage aircraft design.
Source: https://www.centreline.eu/.

Fig. 2. Render of the D8 "Double Bubble" aircraft concept.
Source: Courtesy of NASA https://www.nasa.gov/content/the-double-bubble-d8-0.

Fig. 3. NASA N3-X Turboelectric Distributed Propulsion blended wing-body aircraft concept.
Source: Courtesy of NASA https://www.nasa.gov/content/hybrid-wing-body-goes-hybrid.

For example, the CENTRELINE project was a recent concept validation study for a wake-filling propulsive fuselage aircraft design [8]. This studied a 340 passenger, 6500 nmi range wide-body aircraft (shown in Fig. 1) with a specified entry into service date of 2035. The aircraft aims to reduce CO_2 emissions through the use of a "wake-filling" propulsion design, whereby the momentum lost in the fuselage boundary layer is recovered, or "filled", by using this low-momentum air as the intake air for the propulsion system. This lowers the jet exhaust velocity for the same net thrust and so results in a lower kinetic energy expenditure. This is implemented using a boundary layer ingestion (BLI) fan at the rear of the fuselage. The study compared this to an equivalent reference aircraft entering into service in 2035, where the reference aircraft incorporates 2035 technology but uses a conventional engine arrangement, without the fuselage fan. The propulsive fuselage concept was predicted to reduce CO_2 emissions by 4.6% [8]. The ingestion of the boundary layer by the propulsor at the tail results in highly distorted inlet airflow for the fan, which was evaluated computationally and experimentally as part of the CENTRELINE project. Using simulations of the fluid flow around the fuselage and wind tunnel experiments on a sub-scale model, the inlet airflow profile was predicted. This inlet profile was then reproduced in a low-speed BLI fan test rig using a distortion screen and the fan performance was measured. A second fan, designed with features to mitigate the detrimental effect of the distortion, demonstrated improved efficiency and stability [7]. Other concepts of a similar design include the NASA STARC-ABL [9], Boeing SUGAR FREEZE (https://www.boeing.com/features/innovation-quarterly/aug2017/feature-technical-sugar.page), and DisPURSAL (http://www.dispursal.eu/). DisPURSAL is another European design which was introduced before the CENTRELINE concept where the aft propulsor was powered by a gas turbine in the tail, fed by an s-duct, whereas the others are all turboelectric designs. S-ducts also generate high levels of inlet distortion [10,11] which is then ingested by the engine.

The MIT-Aurora developed D8 "Double Bubble" is a 180 passenger, 3000 nmi transcontinental range concept civil transport aircraft [12], shown in Fig. 2. It is designed for the Boeing 737/Airbus A320 category of operation and incorporates technologies associated with a 2035 year of entry into service. The "Double Bubble" name comes from the two intersecting cylindrical pressure vessels used to form the fuselage into a shape which allows for the inclusion of a lifting nose [13]. The unconventional location for the aircraft's engines, flush mounted in the top surface of the fuselage, between the two vertical stabilisers, means they ingest roughly 40% of the fuselage boundary layer [14]. Boundary Layer Ingestion is an enabling technology for achieving the fuel efficiency levels of the D8 which is estimated to have the potential to reduce fuel burn by 36% compared to a conventional tube-and-wing aircraft [14]. In the same way as with the CENTRELINE concept, boundary layer ingestion reduces the wasted kinetic energy normally in the jet exhaust by "filling-in" the momentum deficit in the fuselage wake. However, the boundary layer growth along the fuselage results in a non-uniform inflow, which is ingested by the intake duct and presented to the engine. This requires consideration as the benefit of BLI may be partially offset by the effect of the distorted propulsor inflow on fan performance. The ONERA Nova is an aircraft concept with a similar fuselage configuration, which also incorporates boundary layer ingesting engines mounted at the rear of the fuselage [15].

The N3-X is a 300 passenger, 7500 nmi range civil transport aircraft concept designed to meet the NASA Subsonic Fixed Wing project 'N+3 generation' fuel burn reduction goal. The airframe is a blended wing-body design where the fuselage forms part of the lifting surface and blends continuously into the wing, as shown in Fig. 3. Two gas turbines with superconducting generators power an array of 14 electric propulsors near the trailing edge of the fuselage. The gas turbine power-generating engines are wingtip mounted to minimise losses and stability issues from inlet distortion. The Turboelectric Distributed propulsion architecture used in this design allows the decoupling of the locations of the power-generating gas turbines from the thrust-generating fans. By incorporating many fans, this generates a very high effective bypass ratio to improve propulsive efficiency and employs boundary layer ingestion while avoiding the ingestion of high levels of distortion into the engine core. Using a Boeing 777-200LR as a reference aircraft, the design was predicted to have a 70% reduction

in mission fuel consumption [16]. Other blended wing-body aircraft designs exist such as the MIT-Cambridge University Silent Aircraft Initiative SAX-40 and the Boeing N2B [5,17]. These use a different engine architecture with pods of embedded "Tri-fans". This is another method by which the effective bypass ratio is improved, where a single gas turbine is connected via shafts to three fans transmitting power mechanically rather than electrically. In an analysis of the SAX-40 propulsion system, de la Rosa Blanco et al. [17] remark that embedding the engines into the fuselage can reduce the installation drag, increase noise attenuation and enable boundary layer ingestion. However, they emphasise that total pressure losses have a significant impact on performance, and there is a large uncertain risk to the design from the effects of inlet flow distortion. Similarly, in the case of the N2B design, flow simulations by Kim and Liou [5] also present the significant effect of inlet flow distortion in the design. In all the above mentioned novel propulsion concepts, the swirl distortion is likely to increase along with the ingestion of a distorted total pressure field. Firstly, the approaching fuselage flow will have some 3-d aspects and therefore will not contain as uniform a swirl distribution as compared to a podded under-wing configuration. Secondly, when an air induction system ingests total pressure distortion, such as a fuselage boundary layer, this augments the swirl distortions generated in the intake duct train [18].

This overview of novel aero-engine architectures demonstrates both the variety and commonality among a range of proposed future aircraft designs. Common features arise among the concepts, such as boundary layer ingestion, lifting-body fuselages, turboelectric propulsion, and the augmentation of fan pressure ratio through electric or mechanical power transfer. An important consideration in the design of the airframes and propulsion systems is the highly distorted and unsteady nature of the inlet airflow. The impact of this flow distortion on the propulsion system stability and performance is further discussed in the following sections.

2.2. Inlet flow distortion phenomenology and characterisation

Inlet flow distortion can arise from a range of aerodynamic aspects such as boundary layer ingestion, lip separation, shock induced separation, vortex ingestion and secondary internal flows [19]. As a consequence, perturbations of total pressure, temperature and velocity are presented to the engine system. This constitutes an element of risk for the development of propulsion systems for future aircraft designs presented in the previous section. Often, these are of concern not only for the aerodynamic efficiency and stability of the propulsion, but also for the effect on the aeromechanical compatibility between the intake and the engine. Inlet distortion is generally classified into three categories: total pressure distortion [20], total temperature distortion [21] and swirl distortion [22]. This section will focus on the sources of the inlet distortion, the phenomenology and the expected impact onto the propulsion system.

2.2.1. Total pressure distortion

Total pressure distortion is the variation in stagnation pressure ingested by the engine caused by irregular flow features upstream of the engine through their effect on the pressure field. The S-16 committee, formed as a working group of SAE International, recognises this distortion type as the predominant destabilising element and often the most common among the different applications [23].

There are multiple sources of total pressure distortion. For example, the shape of the inlet determines boundary layer growth along the inlet walls, possible separation zones, and streamwise vorticity, all of which influence the total pressure of the flow reaching the engine. Moreover, civil aircraft at high angles of attack or cross-wind conditions can develop separation from the lip of the nacelle and a subsequent total pressure decrease in the separated region of the fan face (Fig. 4). Other aircraft configurations with highly integrated propulsive systems are also exposed to wakes and vortices generated by the forebody, nose

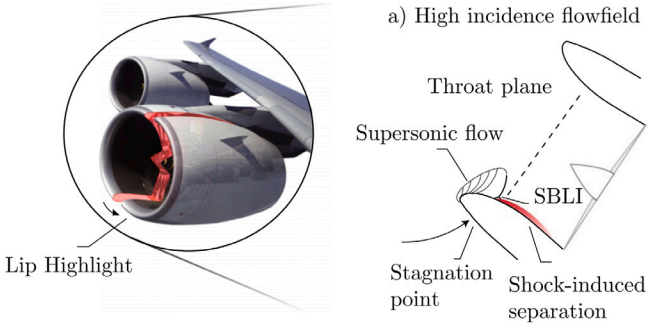

Fig. 4. Inlet total pressure distortion due to intake lip separation at high angle of attack flight condition.
Source: Republished with permission of American Institute of Aeronautics and Astronautics, from [26]; permission conveyed through Copyright Clearance Center, Inc.

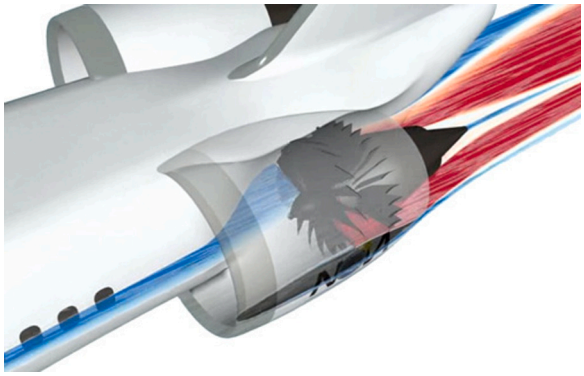

Fig. 5. Boundary Layer Ingestion (BLI) concept NOVA by ONERA [15].
Source: Courtesy of ONERA https://www.onera.fr/en/news/nova-nextgen-onera-versatile-aircraft.

gear, canards and aerodynamic surfaces which may interact with the intake flow and produce flow separations [20,24]. For novel aircraft configurations in which engines are rear mounted and semi-embedded in the fuselage [25,26], the thick inlet boundary layer will generate non-uniform total pressure distributions at the entry of the air induction system (Fig. 5). Due to the shock interactions at the inlet, supersonic aircrafts can also be exposed to total pressure distortions, especially during manoeuvres with large angles of side slip [19]. Devices or excrescences at the intake inlet such as screens to avoid debris ingestion may also cause non-uniform pressure distributions [19].

A number of distortion descriptors were previously proposed to characterise inlet total pressure distortion patterns in industrial intake-engine integration test campaigns. The philosophy behind these formulations was to bring together the pressure data collected by an intrusive pressure rake installed at the interface between intake and engine, or Aerodynamic Interface Plane (AIP), as defined by the S-16 committee in [20,27]. As such, different descriptor formulations were introduced to quantify total pressure variations in the radial and circumferential directions across the AIP ($\Delta P_r/P_{avg}$ and $\Delta P_c/P_{avg}$ respectively, see [27]), whereas aero-engine manufacturers developed additional formulations such as the descriptors based on a critical sector angle θ, as defined by Reid in [28]. This was developed based on the observation that upon increasing the angular extent of the "spoiled" low-pressure region, the effect on the compressor in terms of surge delivery static pressure was dramatic up to a certain value beyond which it stabilised at some minimum value. That point is the critical angle, and the pair of descriptors used with this method are defined by Campbell in [29]. A number of further total pressure distortion descriptor formulations is introduced in the same reference.

Inlet total pressure distortion was previously found to influence the propulsion system efficiency. Results from a turbofan engine test conducted at a ground testing facility with a circumferential inlet distortion pattern showed loss in gross thrust of 2% and specific fuel consumption increased by 6% [27]. More importantly, inlet distortion can also influence the stability limits of the engine. Total pressure losses in the inlet airflow lead to variations in pressure recovery across the engine face which affects the pressure ratio delivered by the compressor behind the distorted regions. The flow physics of how exactly distortion behaves in turbomachinery is an area of active research. However, it is inferred that when total pressure distortion is present, there are regions of high and low total pressure over the rotor face. This means a blade passes into and out of the "spoiled regions" and the blade incidence and, consequently, the blade loading changes as it does so [19]. Depending on the magnitude of the change and on the radial and circumferential extent of the spoiled region, this may cause the blades to stall and may trigger compressor instabilities such as mechanical excitation and, ultimately, compressor surge [30]. This is highly detrimental to efficient compressor operation and very often catastrophic damage can be caused to the hardware as shown by Song et al. [31].

Investigations on the impact of inlet total pressure distortion revealed that both the magnitude and the distribution of the spoiled regions at the compressor fan face play a role in the reduction of the compressor stability margin. Since Reid's experiments on a 6-stage compressor exposed to radial and circumferential distortion patterns, it was inferred that the impact on the compressor surge margin is a function of the area of spoiling [28]. However, the extensive investigations of Melick [32] revealed that the response of the engine to the distortion depends on the length-scale of distortion and compressor chord. This was later associated with the concept of rotor reduced frequency, which was applied to typical transonic compressor fans by Cousins [33]: If the time required for the distortion to travel from the blade leading edge to the blade throat is less than the time for the blade to travel across the distorted sector, the blade response is maximised. This theory is supported by Longley et al. [34]. They observed a severe stability margin degradation when the distortion frequency matched a characteristic speed of the compressor flow field such that the blade exposure time to the distortion became similar to the through-flow time. The reduction in stability margin could be as high as 90% compared to the margin associated with a steady distortion pattern [34]. Therefore, it is concluded that the impact of the total pressure distortion must be evaluated on a case-by-case basis because it is strongly dependent on the response time of the compressor blades. Key references on the matter are collected in Table 1. Additional considerations on unsteady total pressure distortion are discussed in Section 2.2.4.

2.2.2. Total temperature distortion

Total temperature distortions can arise from thrust reverse operation, ingestion of hot gases from firing of armaments or during take-off queues [21]. Total temperature distortion is less investigated than total pressure distortion but nevertheless it can be detrimental to the engine, causing performance degradation, power loss due to engine flame out or compressor instability. This is expected to become more relevant for future formation flight on civil aircraft. Preliminary feasibility studies reported a fuel burn saving of up to 16% for a mid-range passenger aircraft comparable to a A320-200 [45]. Formation flight was recently trialed by Airbus, reporting fuel burn savings of more than 5% on long-haul flights with A350 aircraft [46]. Cases of inlet total temperature distortion were also recorded in helicopter and V/STOL (Vertical and/or Short Take-Off and Landing) aircraft operation when hovering close to the ground [47]. A significant effect on engine stability was observed, especially in cases in which a single distorted region with a considerably large circumferential extent was presented to the engine, rather than multiple distortion sectors [48].

Fig. 6. Tightly-wound ground vortex during taxiing.
Source: The U.S. National Archives.

More investigations are needed to address the total temperature distortion problem and define methodologies for stability assessments. Computational and experimental investigations on this distortion type are limited and this is acknowledged in SAE standard AIR5867 [21]. From the published data, common parameters to characterise temperature distortions quantify the rate of change of temperature variations and also the spatial distribution of the AIP distorted sectors as described in [21].

2.2.3. Swirl distortion

Swirl distortion can be described as the variation of the circumferential portion of the flow velocity vector at the AIP. The development of methodologies to assess the swirl distortion is very recent, since it became clear that the assessment of only total pressure distortion is not sufficient to define the engine's surge margin loss, in cases where swirl distortion is also present [19]. In engine configurations with inlet guide vanes (IGVs) part of the inlet swirl is reduced from the flow approaching the first rotor, which mitigates some of the stability risk linked with inlet swirl. In engines with no IGVs in place, swirl distortion issues may still arise and become detrimental to the engine's stability and performance as described by Cousins in [19]. The source of inlet swirl distortion can be internal or external to the intake. In embedded air induction systems, complex (S-shaped) subsonic diffusers are very frequently used to drive the required amount of flow into the propulsion system. Such diffuser ducts are known to generate large levels of swirl distortion due to the secondary flows which develop because of the curved geometries [49]. Additionally, there have been cases whereby swirl generation originates externally to the intake from various aerodynamic surfaces of the aircraft as described in the relevant SAE standard [22] . In novel aircraft configurations, where the engine is closely coupled and rear mounted, there is an increased likelihood of vortex ingestion from the strakes, leading edge extensions, fuselage and aerodynamic surfaces [22]. For an embedded engine with a convoluted air induction system, the swirl distortion generated within the ducts depends on the total pressure distribution at the inlet such that, for example, the ingestion of a fuselage boundary layer can cause swirl distortions at the AIP [50]. Tightly wound vortices can also be generated by the interaction of the inlet flow with the ground under no wind, head-wind, cross-wind or tail-wind conditions [51], and also during thrust reverser operation (Fig. 6). Moreover, swirl distortion is a concern also in gas turbine intakes for helicopters, in which the inlet flow is subject to the rotor downwash [19]. In turboprop engines and in future hybrid electric distributed propulsion systems, the inlet flow is expected to cause peak swirl fluctuations due to the wake of the propeller blade passing in front of the intake [52].

Similarly to the other distortion types, a number of swirl distortion descriptors were introduced to characterise engine face swirl

Table 1
Experimental (E) and computational (C) studies on engine response to inlet total pressure distortion based on blade resident time theory and total pressure fluctuations.

Distortion type	E/C	Model	Distortion generation method	Key findings	Ref.	Year
Total pressure	E	6-stage axial compressor	Mesh screens for radial, circumferential distortion sectors	Minimum area of spoiling which induces maximum loss in surge pressure ratio	[28]	1969
Total pressure	E	GE, PW, RR rigs and compressors	Mesh screens for circumferential distortion sectors	Stall margin as analytical function of the distortion pattern, distortion level and compressor rotor reduced frequency	[32]	1973
Total pressure	E	Square inlet duct	Random frequency generator with mechanical actuators	Engine responds to unsteady distortion patterns	[35]	1974
Total pressure	C	Parallel compressor model	Steady and dynamic disturbances simulated with analogue computer	Trade-off pulse amplitude vs duration for instability. Steady and dynamic distortion combine linearly for reduction of surge margin	[36]	1977
Total pressure	E	GE low-speed 4-stage axial compressor rig	Rotor mismatch, large tip clearance and mesh screen for circumferential distortion sector	Evidence that compressors have a two natural frequencies associated with modal stall and spike stall	[37]	1995
Total pressure	E	Large scale low speed compressor	Mesh screens for circumferential distortion sector	Severe stability margin degradation if distortion frequency matches a characteristic speed of the compressor flow field	[34]	1996
Total pressure	C	Low-speed compressor	Mesh screens for circumferential distortion sectors	If distortion transport time is less than blade resident time, the blade response is maximised	[33]	1998
Total pressure	E	Ground testing of large scale turbofan engine	Unsteady distortion induced by transient wind gusts	Rotating stall triggered by delay between the response of the inlet and of the fan to incoming fluctuations of low frequency	[38]	1999
Total pressure	E/C	Review of previous work	Experimental and parallel compressor models	Engine response depends on compressor reduced frequency and blade resident time for each configuration	[19]	2004
Total pressure	E/C	Review of previous work	Experimental and parallel compressor models	Very long-length scale disturbances affect rotor in quasi-steady manner while very short ones may not affect the rotor at all	[39]	2010
Total pressure and swirl	E/C	Review of previous work	Unsteady spike-type distortion	Modal or spike-type stall inception. Spike-type stall inception triggered by peak fluctuation of pressure, vorticity, velocity	[40]	2010
Total pressure	C	1/10 RR transonic axial fan stage	Step, 1 pulse, continuous pulses of total pressure	Trade-off pulse amplitude vs. duration for instability. Fan less tolerant to continuous stream of pulses rather than single one	[41]	2015
Total pressure	E	Subsonic axial flow fan stage	Mesh screens for radial distortion sectors	Stall inception occurs mainly through long-scale disturbances with embedded spikes. Inflow distortion amplifies spikes	[42]	2017
Total pressure	E	NASA GRC 8 × 6' wind tunnel for BLI tests	Thick boundary layers	BLI-type inlet distortion can excite natural frequencies of the fan rotor	[43]	2019
Total pressure	C	Transonic axial-flow fan stage NASA R67	Circumferential distortion sector	Stall inception triggered by periodic tip leakage flow of the blade encountering distortion. Longer exit ducts worsened engine stability	[44]	2019

patterns. A first set of formulations was initially shown by Sheoran and Bouldin [53], based on swirl-angle data at the AIP using the engine rotation direction as the positive direction. These formulations include expressions to characterise Sector Swirl (SS), Swirl Intensity (SI), Swirl Directivity (SD), and Swirl Pairs (SP) at an AIP. The mathematical definitions of the four swirl distortion descriptors are given in Sheoran and Bouldin [53] along with examples of descriptor values for a variety of swirl patterns. The SAE Aerospace information Report AIR5686 [22] gives more in-depth examples with example calculations for representative cases.

Swirl distortion has not previously attracted as much attention as total pressure distortion, and the impact on the aero-engine is still relatively poorly understood. Initial studies used velocity triangle based assessments to quantify the influence of swirl patterns on axial compressors [22]. Some studies showed that the vibratory response due to unsteady swirl can be equally severe as total pressure distortion and can excite the blade resonant frequencies [54–57]. Vortex flows can also set up harmonic effects in the flow field that drive high-cycle fatigue leading to reduced operational lifespan of the engine [19]. More recent studies assessed the swirl distortion in the form of tightly-wound discrete vortex and paired swirl, for example in the case of ground vortex ingestion or S-shaped intakes swirl distortion, respectively. Mitchell [58] demonstrated that the impact of discrete wing-tip vortex ingestion depends on many parameters including the vortex ingestion position relative to the intake inlet, the vortex strength, the swirling direction and the trajectory from inlet to fan face. The highest loss in surge margin was for counter-swirling vortices near the hub, which caused a loss in surge margin up to 6% for relatively high rotor speed [58]. In a more recent computational work, Mehdi [59] demonstrated correlations between the swirl angle and the loss in compressor surge margin for bulk, single and multiple vortex ingestion. Based on his CFD simulations, the reduction of surge margin caused by a single vortex was relatively greater than the one caused by multiple or bulk vortices [59]. Key references and findings on the response of aero-engines to swirl distortion are collected in Table 2.

2.2.4. *Unsteady distortion*

For many years, unsteady variations of total pressure, swirl or temperature distortion were considered of low importance despite some earlier suggestions made in the 70s to include the time-variant element of inlet total pressure distortion in the characterisation of an engine's

Table 2
Experimental (E) and computational (C) studies on engine response to inlet swirl distortion.

Distortion type	E/C	Model	Distortion generation method	Key findings	Ref.	Year
Swirl	E	J-85 engine	Wing tip vortex ingested in S-duct intake	Vortex impact is function of ingestion position, vortex strength, swirling direction and trajectory	[58]	1975
Swirl	E	Review of previous work	Canards wing tip vortex, swirl induced by S-duct intakes	Total pressure distortion not adequate to define stability limit if swirl distortion is present	[54]	1982
Swirl and total pressure	E/C	Review of previous work	Experimental and CFD models	Vibratory response to swirl can be more severe than total pressure distortion	[55]	1997
Swirl	C	Transonic axial fan stage NASA R67, high-pressure compressor stage NASA R37	Bulk and tightly wound vortices	Correlation between swirl descriptors and loss in surge margin. Greatest surge margin loss for the ingestion of co-rotating vortex near the hub	[59]	2014
Swirl and total pressure	E	Transonic axial fan stage NASA R67	Tip-radial and hub-radial total pressure loss. Co- and counter-bulk swirl	Superposition of radial total pressure and bulk swirl distortion is not valid to predict compressor stability	[60]	2016
Swirl and total pressure	E/C	Review of previous work	Bulk, paired and multiple swirl in parallel compressor models and experiments	Impact of combined paired swirl and total pressure distortion is not predictable with superposition of effects	[22]	2017
Swirl	C	Transonic high-pressure compressor stage NASA R37	Bulk swirl and paired swirl with IGVs	Bulk swirl more predictable than twin swirl. Need to consider unsteady flow to predict stall margin	[61]	2018

stability degradation [62]. Hence, limited effort went into understanding their nature and their influence on an engine's performance and stability penalties [63]. As a result, large engine development campaigns focused only on evaluating the impact of steady-state distortion patterns on the propulsion system. In order to reproduce such patterns at engine test-beds, various methods were applied, mostly based on the imposition of distortion profiles, generated by appropriate screens installed forward to the AIP [63]. However, it was soon realised that engine surge events could neither be reproduced nor predicted via a time-averaged, steady-state picture of inlet distortion, which supported the hypothesis that time-dependent distortions may have large effects on the engine's stability limit [63]. In fact, the unsteady part of the distortions was found to add as much as 30% range to the steady-state measurements [19]. These peak fluctuations were considered large enough to impact engine performance and stability.

Although the engine response to unsteady inlet distortion is not fully understood, many researchers demonstrated that unsteady flow fluctuations can trigger stall inception mechanisms in aero-engine compressors. The experiments of Longley et al. [34] were among the first to identify two mechanisms which are associated with the stability margin degradation of the engine: modal stall and spike stall inception. The first is associated with long length-scale distortions with a signature frequency at about 30% of the rotor speed [34]. The second is associated with short and localised disturbances at about 70% of the rotor speed [34]. While modal stall usually occurred because of the whole compressor system instabilities, the spike-stall is much more common especially in modern, highly loaded compressors because it can be triggered by localised peak fluctuations of pressure, vorticity, and velocity [40]. In the context of spike-type disturbances, some researchers investigated the impact of unsteady fluctuations of total pressure. One of the first studies by Wenzel and Blaha [36] involved the generation of pulses with an analogue computer which fed steady and dynamic disturbances to a parallel compressor model. It revealed that there was a trade-off between pulse amplitude and pulse duration which generated instabilities [36]. Interestingly, this study also demonstrated that steady and dynamic distortion combined linearly for the reduction of surge margin [36]. These conclusions were verified by a recent CFD study by Shaw [41] of a transonic axial fan stage which was exposed to step-like, single and multiple total pressure pulses. The trade-off between pulse amplitude and duration was verified, and it demonstrated that a range of pulse duration between 20% and a full rotor revolution can stall the fan depending on the operating condition of the compressor. Moreover, the fan was less tolerant to a continuous stream of pulses rather than a single one [41]. Latest studies on the spike-type distortion showed that spikes are also embedded in long-scale disturbances due to inlet total pressure distortion and that severe inlet distortion amplifies the likelihood of spikes [42]. Similar conclusions are also drawn by Zhang et al. [44] who reported that stall inception is triggered by the periodic leakage flow of the blade encountering the distortion. More recent computational and experimental studies for a modern low pressure ratio transonic fan have also identified the impact of unsteady total pressure distortions on the rotating stall cell inception, rotation speed and extent [64].

A certain level of effort was recently made to include unsteady total pressure distortions into engine industrial testing and apply extreme value statistics to reduce testing and computational requirements for quantifying its effect [65]. The SAE S-16 turbine engine inlet flow distortion committee recently acknowledged the importance of unsteady pressure distortion and classified them under the definition of planar waves [66]. These are one-dimensional, unsteady pressure fluctuations at the compressor face. Planar waves can be generated internally within the inlet in the case of flow separations, shock-boundary layer interactions, supersonic flight buzz, un-start or interactions with adjacent engines. These can be also linked to instabilities developed during subsonic flight at low mass flow ratio or the response to inlet control system inputs during supersonic flight. Additional external causes may trigger these fluctuations, such as vortex ingestion, ingestion of wakes from nose gear and bomb bay doors, atmospheric gusts and explosions, and armament firings. The occurrence of unsteady distortions is not restricted to extreme manoeuvres, but instead, may appear also in the normal flight envelope [66], and thus this is an element of risk for the engine stability during normal flight conditions. Although the SAE standard AIR5866 [66] summarises a number of methodologies to assess planar waves, there is no evidence yet related to the sensitivity of the engine to these unsteady oscillations. Often, this distortion is addressed through several iterations between engine manufacturers and airframe designers where design modifications are made to avoid or suppress the generation of such planar waves as described in [23].

Overall, it is concluded that there is no general rule to predict the engine response for different unsteady total pressure distortion patterns, amplitudes and frequencies. Previous work suggests a typical range between 1-per-rev and blade passing frequency for disturbances that could contribute to the instability of a compression system. Alternatively, for axial compressors, a circumferential spoiled sector of 4–5 blades can also generate instability. However, this must be evaluated on a case-by-case basis as it can be affected by a range of parameters even low frequency ambient wind perturbations of less than 5 Hz [38]. Since instabilities such as spikes are localised in the blade spacing, many flow features such as boundary layers, tip leakage and blade wakes can play a role in compressor instability. Furthermore, the nature of these

instabilities can be pressure, vorticity, and velocity fluctuations [40] and overall the phenomenon is still not well understood. Nevertheless, the importance of unsteady distortions is now widely acknowledged within the relevant community along with the necessity of more advanced experimental and data analysis methods, to be able to provide richer flow field data in space and time. Such advancements will play a critical role in improving the current understanding of complex, highly unsteady distorted flows and will eventually support the development of design rules for closely integrated aircraft and engine systems.

2.2.5. Combined distortion

In most configurations, the presence of one type of inlet distortion is not exclusive and more than one distortion type can co-exist at the fan face, which can further deteriorate the engine's stability margin as described in [22]. For example, wakes from bodies upstream the intake can generate a wide range of combined swirl and total pressure distortions [67]. Moreover, previous observations suggest that new engine developments may require the characterisation of combined pressure and temperature distortions [68]. Accountability of combined total pressure distortion and planar waves should be also in place for engine stability assessments [66]. The SAE guidelines recommend that when considering combined distortions, it should be verified that the superposition of effects is appropriate for modelling the combined effect of distortion types on the engine stability, and this should be evaluated on a case-by-case basis [66]. For example, it is believed that total pressure and total temperature do not interact with each other and thus the superposition of effects is granted [21]. However, Naseri et al. [60] demonstrated that the superposition of total pressure and swirl distortion can only be linked to compressor performance and less to compressor stability. The complexity around combined distortions is also acknowledged by other researchers who highlighted the need to include both sources of steady and unsteady distortion for the understanding of stability limits and mechanical forced excitation on the compressor blades [54–57]. During the engine operability considerations a key concern related to unsteady distortions is the non-synchronous blade forcing that these can cause. However, no solid guidelines exist regarding testing and simulation with combined distortion effects primarily due to the lack of understanding of such flow mechanisms and hence the inability to link these with engine performance and stability penalties.

2.3. Current industrial practices in distortion measurements and knowledge gaps

Current practice for inlet distortion measurements in industry includes the use of a number of intrusive pressure rakes at prescribed positions at an engine's AIP as shown in [27]. An example of such a distortion rake installed inside an intake duct is shown in Fig. 7. These pressure measurements are most commonly of low temporal resolution, although time-dependent rakes were also shown previously in selected cases where time-resolved data was required [69]. The ARP1420 aerospace standard [27] prescribes pressure probe locations across an AIP, to ensure representative data acquisition, without missing significant flow details and without causing too much blockage. Alternative intrusive methods include the use of miniature high-speed pressure transducers embedded in rake arrays to minimise blockage effects. This allows unsteady pressure measurements across an engine face plane as well as in turbomachinery passages [33].

Although pressure probes have the disadvantage of being intrusive to the flow, these systems can capture data at very high temporal rates in the order of >10 kHz or also provide swirl characteristics [69]. These systems include multi-hole probe arrays able to capture flow angularities as well as total pressure variations across the plane of interest. Very often, only a small number of multi-hole probes is available during a certain test campaign hence the rake on which they are mounted has to be traversed across the measurement plane as

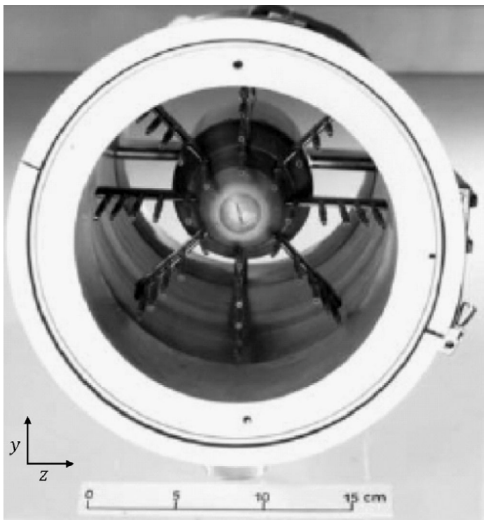

Fig. 7. Pressure rake used for total pressure distortion characterisations.
Source: Reproduced from [69].

indicated in [7]. In such cases, the acquired information is no more synchronous in time across the plane and, hence, only time-averaged distortion measurements can be obtained without acknowledging the unsteady part of it. This was often found to provide misleading information about the flow non-uniformities, whose mean values were significantly lower than instantaneous peak events that could trigger engine instabilities [70,71].

Although the standards prescribing the total pressure distortion measurement methods have existed for many decades [20], recommended practices about swirl measurements have only recently been introduced [22]. However, it is easily realised that, although unsteady total pressure and swirl distortion was historically identified as a key detrimental factor to an engine's stability, the relatively low maturity of advanced flow measurement methods in combination with the high complexity of more sophisticated measurement systems, has limited the understanding of the complex, unsteady flows linked with advanced air induction systems. Numerous historic examples reinforcing this statement were previously reported and comprehensively summarised in [72]. A key message from this work focuses on the fact that the poor characterisation of the unsteady part of the various types of distortions along with the inability of existing measurement techniques to synchronously measure more than one type of dynamic distortion, yields poor interpretation of the influence of such complex flows on engine stability and the loss of surge margin. This was acknowledged as a major pitfall in some previous engine development programmes such as the YF-12, the F-15, F-18 and F-22 among others [72]. Some further emphasis was given to the currently insufficient capability to capture unsteady total temperature distortions at a sufficiently high temporal frequency pertinent to engine response [21]. As such, the necessity for richer data primarily in space but also in time, to aid the understanding of these complex distortions that lead to engine failure events remains a key requirement. The timeliness of such developments is now more critical than ever as an era of closely coupled aircraft-engine systems emerges in both the civil and defence markets, whose development and engine integration risks cannot be easily mitigated by current practices. Imaging based laser-optical flow measurement techniques have the potential to address this limitation by providing flow data of particularly high resolution in space and time. Recent work suggested that optical velocimetry techniques such as Particle Image Velocimetry (PIV) deliver a spatial resolution of cross-flow velocity measurements by at least one order of magnitude greater than conventional intrusive distortion measurement methods [73]. As such, a currently open

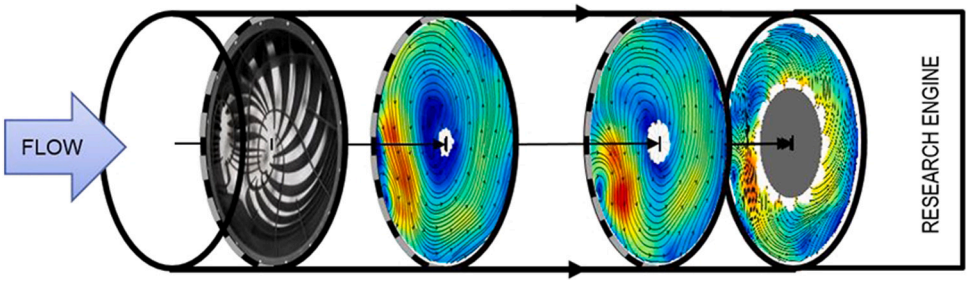

Fig. 8. Example visualisation of the mean secondary flow behind a customised distortion screen measured with S-PIV inside Virginia Tech's full-scale engine research rig. Colours represent secondary flow magnitudes (red large, blue small) and streamlines the local flow direction.
Source: Republished with permission of Emerald Publishing Limited, from [74]; permission conveyed through Copyright Clearance Center, Inc.

research question is now emerging about the development and application of non-intrusive, optical methods for the characterisation of unsteady distortions in novel air induction systems aiming to further educate the development of stall tolerant, closely coupled propulsion systems. An additional question is related with the applicability of such non-intrusive methods at in-flight tests which were previously found of critical importance in certain development programmes, due to the inability of ground- or wind-tunnel test campaigns to capture extreme, instantaneous distortion events [72]. Overall, it is anticipated that the application of non-intrusive, laser based flow diagnostics for unsteady inlet flow distortions at ground but also in in-flight test campaigns, is one of the most promising routes to address the design challenges associated with the development of the next generation, closely coupled, aircraft architectures.

3. Non-intrusive distortion measurements; current achievements and future outlooks

3.1. State-of-the-art in non-intrusive distortion measurements

To capture the full range of the various types of inlet flow distortion and determine their impact on the stability and performance of a propulsion system, measurements of static pressure, temperature and three-component (3C) velocity are required. Given the known limitations of currently used intrusive distortion measurement methods (low spatial and temporal resolution, intrusive instruments that interact with the flow), existing technologies are inadequate to sufficiently reduce the risk on the development of future closely coupled engine-airframe configurations. In the context of swirl distortion measurements, planar laser-optical techniques such as Particle Image Velocimetry (PIV) and Doppler Global Velocimetry (DGV) have demonstrated their ability to spatially resolve complex flow patterns and capture the associated unsteady characteristics.

The PIV technique enables flow velocity measurements in a two-dimensional plane by illuminating small tracer particles added to the flow and capturing two images in quick succession, subsequently using computational methods to determine the displacement of particle patterns between the two images. Stereoscopic PIV (S-PIV) extends this method by using multiple cameras to capture flow velocity in three dimensions, across a given flow plane [75]. The application of S-PIV methods for cross-flow swirl distortion measurements in civil intake configurations was previously demonstrated by Hoopes [76] and Guimaraes-Bucalo et al. [77], who also developed a method to prescribe swirl distortion patterns at the inlet of a propulsion system via tailored made distortion screens. The resulting distorted inlet flow fields were investigated in several studies at a small scale rig and a full scale engine test facility [77–81]. Example flow fields measured with S-PIV at different axial stations behind the distortion screen are presented in Fig. 8. Previous work at Cranfield University focused on S-PIV measurements in convoluted subsonic diffusers [70,73]. Therein, the superior spatial and temporal resolution of the resulting PIV velocity

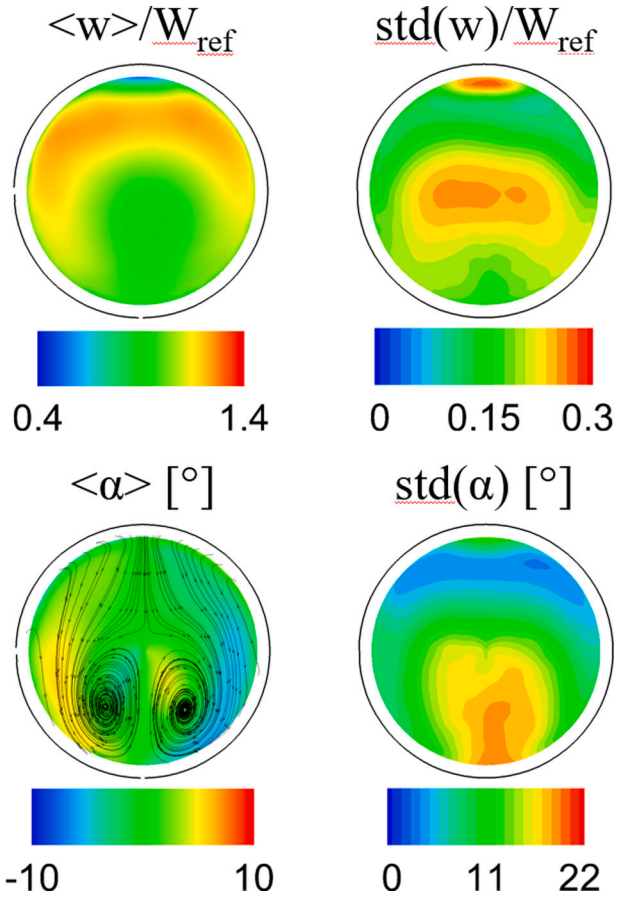

Fig. 9. S-PIV measurements of time-averaged (⟨⟩) and unsteady (standard deviation, std()) streamwise velocity component (w) and swirl angle (α) downstream of an S-shaped diffuser [18].

fields was exploited to highlight flow unsteadiness associated with the swirl angle, whose fluctuations (highlighted by the standard deviation, std(α)) could double the time-averaged distortion levels (Fig. 9). This work was further expanded by high-speed S-PIV velocity measurements at repetition rates of up to 8 kHz. Proper orthogonal decomposition (POD) analysis was used to identify the most energetic unsteady structures and the frequency content of the unsteady distortion descriptors was analysed with a spectral analysis [18,71] (Fig. 10). The high temporal and spatial resolution of high-speed S-PIV enabled also more advanced analysis methods for tracking unsteady localised distortion events presented to the engine [50].

Doppler Global Velocimetry (DGV or Planar Doppler Velocimetry — PDV) methods were introduced in the early 90's by Meyers and Komine [82,83]. Similar to PIV, the flow is seeded with small particles

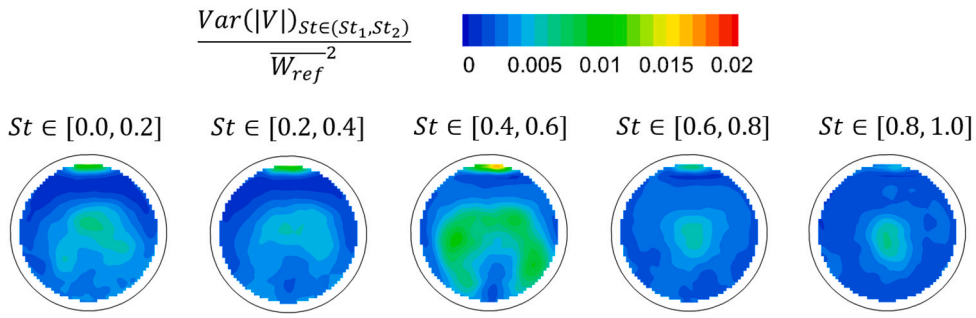

Fig. 10. Spectral signature of the streamwise velocity downstream of an S-shaped diffuser [18].

and illuminated with a thin laser sheet. However, instead of analysing the particle pattern displacement between two consecutive frames using correlation techniques, in DGV, the Doppler frequency shift of the light scattered from particles moving through the measurement plane is transformed into a detectable intensity change by means of molecular absorption. In the context of inlet flow distortion, the DGV method was successfully used to derive the time-averaged swirl distortion inside the intake duct of a fighter aircraft model [84]. These measurements were conducted at the DNW NWB[1] wind tunnel facility in Brunswick, Germany. A half-model of the aircraft was attached to a six-degree of freedom positioning system inside the wind tunnel's open jet test section and an aspiration system was used to model compressor suction, enabling the simulation of a large set of test conditions in terms of mass flux, angle of attack and yawn angle, as shown in Fig. 11. From the diagnostics point of view, the main technological hurdle was the anticipated usage of DGV to measure flow velocities inside the aircraft models convoluted intake duct. The resulting optical accessibility constraints were addressed by replacing a segment of the intake duct with an optical module. Thereby, the AIP was consecutively illuminated with laser light from three directions using miniaturised light sheet optics, which were supplied with laser light via 15 meter long optical wave guides. Observation occurred through an optical probe located three tube diameters downstream from the measurement plane and an imaging fibre was used to transfer the imaged scene to the DGV camera system. The contour plot in Fig. 11 shows a sample flow field obtained with the described system, exhibiting a characteristic asymmetry of axial velocity and a dominating eccentric vortical structure rotating in counterclockwise direction.

Even though notable progress in the diagnostic capability to characterise inlet flow distortion has been accomplished, laser-optical measurement techniques such DGV or PIV require the use of tracer particles, which comes with a number of caveats, including the fouling of the optical access as well as the requirement of a uniform seeding distribution across the measurement plane and the installation of seeding rakes within the intake sub-system, posing particular challenges for airborne measurements. In addition, DGV is prone to measurement bias caused by multiple scattering in densely seeded flows [85,86].

Aside from seeding related issues, the application of the PIV technique requires uninterrupted optical accessibility to the test section, which might not be available in ground test scenarios with more complex intake geometries and will certainly not be feasible for in-flight application. Instead, flexible probe-based measurement solutions will be required. Some examples of probe-based PIV, relying on observation with rigid borescopes exist in the literature [87–89]. But these devices lack flexibility to be adapted to complex geometries and the optical resolving power of instruments relying on flexible imaging fibre technology, is insufficient to resolve discrete particles as required for PIV [86,88]. Therefore, the intensity based DGV method has a clear advantage for probe-based applications since the technique's underlying principle does not require high-quality imaging of small objects such as μm-sized particles, but instead analyses the Doppler-shifted light scattered from an ensemble of particles detected at the respective resolution element [86]. In addition, DGV potentially has access to all three velocity components with just a single camera view, whereas PIV requires a stereoscopic camera arrangement to capture both the two in-plane and the out-of-plane velocities.

Although DGV has demonstrated the ability to achieve fully probe-based measurements of the mean three-dimensional velocity field in complex experimental scenarios, the aforementioned approach lacks the required time resolution to handle the unsteady flow regime at the AIP. To date, only few DGV approaches to measure flow velocity at high acquisition rates of several kHz have been presented [90,91]. These methods rely on avalanche photodiode or photomultiplier tube arrays for signal detection and, thereby, trade the capability to resolve large coherent flow structures for time resolution. Recently, time-resolved DGV measurements of a single velocity component in a supersonic heated jet were achieved at 50 kHz repetition rate by combining high power continuous wave (CW) laser illumination with high-speed camera technology [92].

Even though recent progress was accomplished, the characteristics of continuous wave laser light sources are the main limiting factor for time-resolved *and* large-field measurements with DGV. For these lasers, the scattered intensity per resolution element is small so that camera exposure times are typically on the order of 10 to 20 ms [84], which is too long to capture flow dynamics in the Mach number range relevant to intake flows. To perform whole-field measurements with DGV resolving the relevant time and spatial scales, pulsed laser sources would have to be used. Several studies applied pulsed frequency tunable injection-seeded Nd:YAG lasers to acquire instantaneous velocity information with DGV [93–95]. A major concern with these systems is a spatial variation of laser frequency within the light sheet, which is varying from pulse to pulse and can reach values of up to 100 MHz, potentially resulting in velocity errors of tens of meters per second [93,96,97]. To achieve the necessary temporal resolution to capture the unsteady aerodynamics at the AIP, novel pulsed laser concepts with enhanced spectral quality are required.

In summary, the state-of-the-art in swirl distortion measurement has been significantly expanded by laser-optical PIV and DGV methods, from a few intrusive probe measurements to whole-field unsteady flow characterisation. While PIV has clear advantages in terms of capturing the unsteady component of swirl distortion, DGV shows great potential for experimental scenarios with aggravated optical accessibility. However, in light of the above limitations concerning flow seeding, optical accessibility for PIV and time resolution for DGV, it is questionable whether the capabilities of both methods can be made available for the entire engine development cycle from ground testing to in-flight experimentation and certification. Moreover, both PIV and DGV lack the ability to capture scalar flow quantities and, thus, total pressure and temperature distortion is left out of the picture. For further detailed information on the previously discussed measurement techniques, including error characteristics and limitations, we refer to work outlined in [75,98].

[1] German–Dutch Wind Tunnels, Niedergeschwindigkeits-Windkanal Braunschweig.

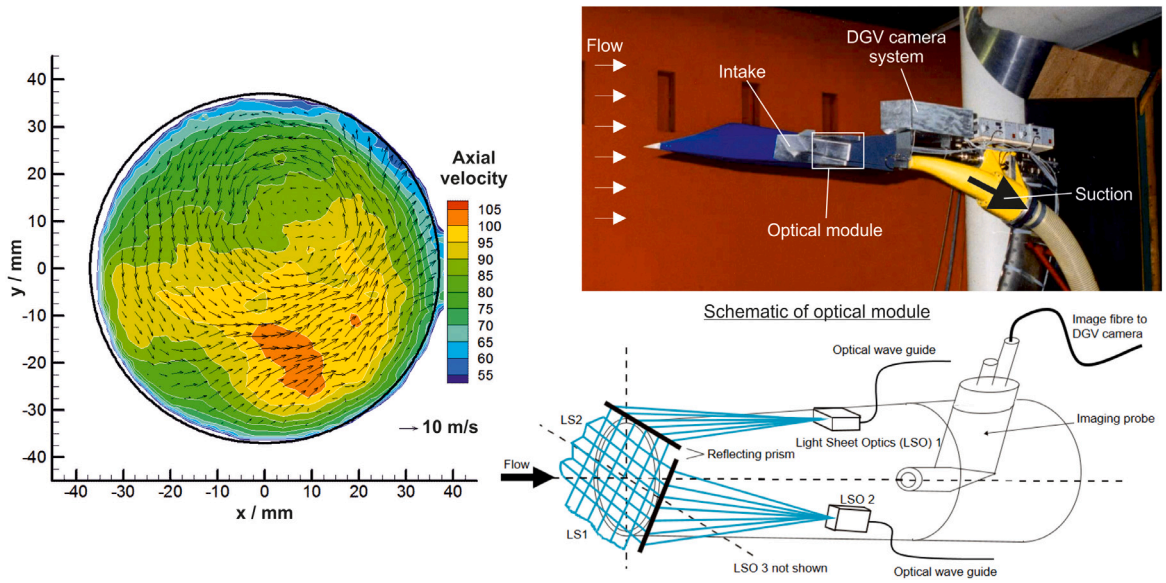

Fig. 11. The photograph (upper right) shows the investigated fighter aircraft half-model mounted on a six-degree of freedom positioning mechanism. The inlet duct is connected to the aspiration system (yellow segment and hose on the right). DGV camera system and associated electronics are mounted behind the aircraft model (metallic grey boxes). Optical wave guides and an imaging fibre (grey bundle on top of yellow bend) are used to deliver laser light to and transfer the measured signal from the measurement plane. A schematic overview of the optical module is provided below and a measured time-averaged velocity field is shown on the left [84].

3.2. Non-intrusive seeding-free measurement techniques for complex internal flows

The successful application of optical flow diagnostics to measure velocity, static pressure or temperature in air flows, by adding neither particles scattering light in the Mie regime (diameters between 1 and 100 μm), nor seeding tracer molecules such as acetone, toluene or nitrogen oxide, is a challenging task. Since the scattered light intensity scales with the scattering cross section, which is several orders of magnitude higher for particle scattering compared to molecular scattering or fluorescence, powerful lasers and sensitive detectors are required to apply these molecular techniques. Owing to the different photophysical mechanisms involved, the following overview of non-intrusive seeding-free measurement techniques is further subdivided into three families: Laser Induced Fluorescence (LIF) methods, methods utilising molecular tagging and methods relying on molecular scattering. The section concludes with a final comparison and evaluation of the presented techniques, with respect to their qualification of characterising inlet flow distortion.

LIF methods

In Laser Induced Fluorescence (LIF) methods, the emission wavelength of a laser has to be aligned to an occupied electronic state of a single atomic or molecular species, such that a higher energy level is excited by absorbing part of the incident radiation. After a specific upper state lifetime, the excited molecule relaxes back to its ground energetic state, with a certain probability of emitting a fluorescence photon. The LIF signal can in principle be used to measure number density, temperature, species concentration, the velocity component along the laser propagation direction and pressure [99]. Without the addition of tracer molecules, the usage of resonance techniques such as LIF methods must rely on the natural constituents of air. In this context, only O_2 (oxygen) and CO_2 (carbon dioxide) possess absorption lines that can potentially be probed with available laser light sources to derive the relevant flow quantities in applications of practical relevance.

O_2 LIF. In oxygen LIF, transitions in the Schumann-Runge absorption system near 193 nm [100] or 248 nm [101] are excited with ArF (argon fluoride) or KrF (krypton fluoride) excimer lasers. The resulting fluorescence emission spans a wavelength range in the UV (ultraviolet) from 200 to 450 nm with about 70% of the power between 220 and 280 nm [100]. Since excitation as well as detection occur in the UV, this sets aggravated requirements to the quality of the optical access. Likewise, camera sensors are typically insensitive in the UV spectral range, so that image intensifiers have to be used for imaging applications.

Under AIP relevant flow conditions, populated ground state transitions are excited to the oxygen B-state, which lies above the dissociation energy of O_2, leading to a very short upper state lifetime of a few picoseconds only [100]. The consequences of the short upper state lifetime are summarised by Miles and Lempert [102]: Due to the rapid depopulation of the upper state the emitted fluorescence is almost independent of collisional (pressure) quenching. The fluorescence yield is proportional to the number of excited molecules and, thus, density measurements at constant temperature or vice versa are feasible in principle. However, since the major part of the absorbed laser energy is lost to predissociation and only 0.004% of the excited molecules fluoresce, resulting LIF intensities are very weak. Finally, the short lifetime leads to an increased natural broadening of individual absorption lines (FWHM > 100 GHz), so that a Doppler shift caused by flow velocity of several tens to hundreds of MHz cannot be distinguished from the fluorescence emission spectrum. To date, the potential of O_2 LIF to be applied to aerodynamic flows as a point measurement technique was only explored in laboratory scale studies [103–105]. As a remark, since at higher temperatures additional vibrational states emitting stronger fluorescence signals are thermally populated [102], so called hot oxygen LIF was introduced as a planar technique for flame studies [106,107].

Co_2LIF. Laser induced fluorescence of carbon dioxide based on IR (infrared) radiation is a promising approach to measure pressure, temperature or flow velocity in flows with CO_2 content. The 532 nm output of a Nd:YAG nanosecond-pulse laser was used to pump a wavelength tunable OPO (Optical Parametric Oscillator) to excite CO_2 vibrational transitions near 2.0 μm in [108]. Since the resulting fluorescence emission occurs in the infrared at 4.3 μm, a liquid nitrogen cooled IR sensitive InSb (Indium Antimonide) camera was used for detection. A single-pulse example CO_2 LIF image is shown in Fig. 12. A strong quenching effect of N_2 and H_2O on the CO_2 fluorescence was identified, so that linear excitation was deemed appropriate for qualitative

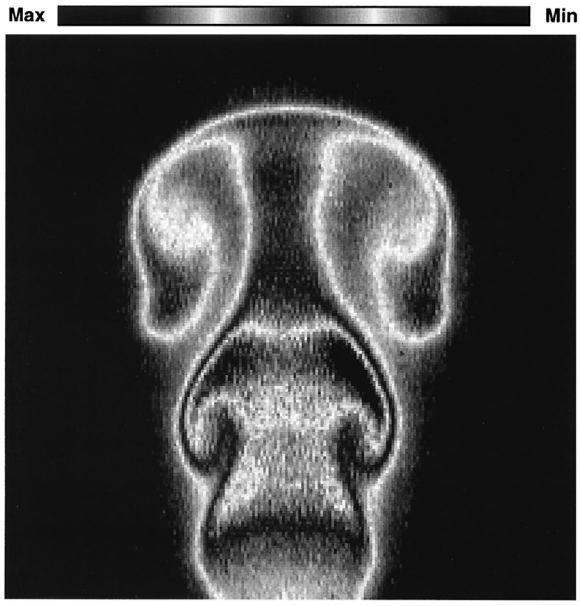

Fig. 12. Example CO_2 LIF visualisation of a 6-mm-diameter forced CO_2 jet at room-temperature mixing with ambient air. The fluorescence signal is excited with a 8 mJ pulse at 2.0 μm and an InSb camera collects fluorescence at 4.3 μm.
Source: Reprinted with permission from [108].
© 2002 The Optical Society.

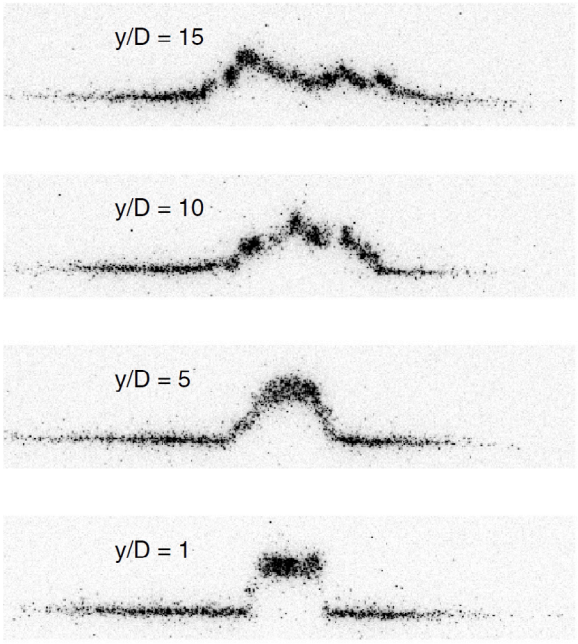

Fig. 13. Single-shot images of displaced FLEET lines at different downstream locations corresponding to heights above the jet exit of 1, 5, 10, and 15 mm. Fluorescence is collected 2 μs after the tagging laser, and the camera gate width is 1 μs. The unperturbed flow position is indicated by the fluorescent lines outside of the free jet.
Source: Reprinted with permission from [115].
© 2011 The Optical Society.

visualisation only. The same authors used an identical camera setup, combined with a CO_2 laser generating laser pulses at 10.6 μm of 5 J pulse energy and 2 μs length, to realise a saturated excitation scheme [109]. The method was successfully applied to visualise a transverse CO_2 jet in a laminar co-flow as well as the CO_2 content of a CO/H_2 diffusion flame with a large field of view of 11 x 11 cm^2. The collected LIF signal was found to be proportional to CO_2 mole fraction and a minimum detection limit of about 1000 ppm could be achieved. In a first effort to provide quantitative results by means of the CO_2 LIF technique, the saturated approach was applied to measure time-averaged temperature and pressure fields in an under-expanded jet consisting of 30% CO_2 and 70% N_2 issuing into a 300 mbar nitrogen ambient atmosphere [110]. Similar to [108], an optimised Nd:YAG pump laser OPO combination with an output energy of 75 mJ was used to excite the saturated CO_2 LIF signal. A small sheet of 12 mm height was formed and the laser wavelength was consecutively tuned to two absorption lines near 2 μm. From the ratio of the respective LIF signals, time-averaged temperature and pressure fields were derived.

A different approach with the potential to derive concentration, temperature, pressure as well as velocity information from a CO_2 LIF signal was introduced in [111]. The concept is based on wavelength scanning the output of a CW quantum cascade laser emitting IR radiation at 4.3 μm across an appropriate absorption line. The integrated LIF signal below the resulting lineshape scan is a measure of CO_2 concentration. Furthermore, the ratio of the integrated signals of two neighbouring absorption lines can be used to derive temperature. Also, the gas pressure is calculated from the collisional width obtained from fitting a lineshape model to the scanned absorption line and flow velocity can be inferred from a bulk Doppler shift of the absorption line. Since fluorescence emission and absorption occur at the same wavelength range, the CO_2 LIF signal is prone to fluorescence trapping and the optical path through the absorbing medium has to be kept short to minimise its influence. To prove the concept, planar pressure and concentration fields were measured in a CO_2-Ar jet in Ar co-flow by expanding the laser into a small sheet of 5 mm height. Due to superior SNR (signal-to-noise-ratio) compared to previous approaches, the CO_2 detection limit was lowered to 200 ppm in the planar measurement configuration, which is potentially sufficient for applications in dry standard air (~400 ppm).

Molecular tagging velocimetry

The term Molecular Tagging Velocimetry (MTV) describes a group of laser-optical techniques based on the excitation of a long-lasting fluorescence signal along a laser beam from molecules naturally present in or introduced into the flow of interest. The velocity of the molecules is determined by detecting the fluorescence of the tagged line at two consecutive instants within the radiation lifetime of the tracer and by measuring the shift of the fluorescence pattern between the images [98, 112]. The method can be extended from a one-dimensional single-component velocity measurement to the full 3C velocity vector field by writing a crossed pattern of fluorescence lines and by stereoscopic imaging of the pattern displacement [113]. However, most MTV methods require the addition of molecular tracers to supply the required luminescent properties and to date, there are only two techniques which have the capability to be applied to unseeded air flows. The so-called RELIEF (Raman Excitation and Laser-Induced Electronic Fluorescence) technique involves the usage of three laser wavelengths [114] and, thus, is too complex to be applied to flows of practical interest. Consequently, only the FLEET (Femtosecond Laser Electronic Excitation Tagging) method will be further outlined.

FLEET. The FLEET technique is a non-intrusive laser diagnostic method to measure flow velocity in nitrogen containing gas flows introduced by Michael et al. in 2011 [115]. In this work, a femtosecond laser with a pulse width of 120 fs and 1.2 mJ pulse energy, emitting laser light at 810 nm with 10 Hz repetition rate is directed onto the examination area above a high velocity air jet. The very short pulse results in high irradiance at the laser focus, so that nitrogen molecules dissociate into atomic nitrogen. When the nitrogen atoms recombine to N_2, a long-lived fluorescence signal in the spectral range between 560 to 660 nm is emitted, tagging the flow along a line of ~1 cm length. A single component of flow velocity is finally obtained by imaging

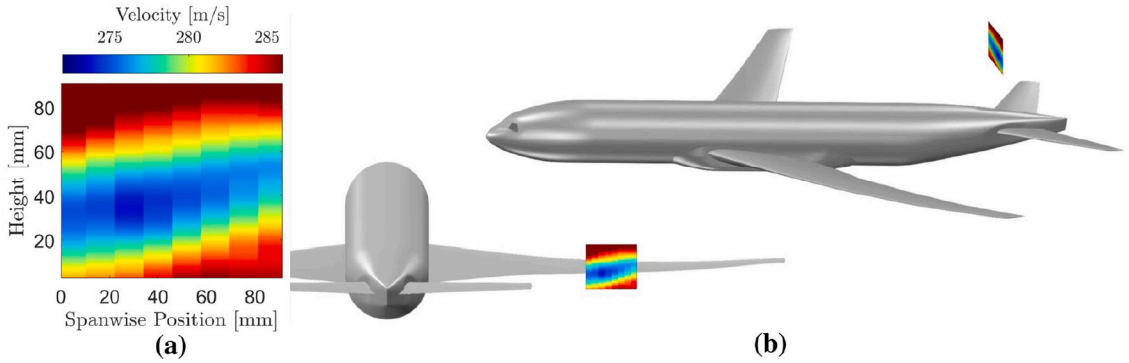

Fig. 14. FLEET measurements in the wake downstream of the CRM wing. A motorised mirror was used to scan the laser beam to eight different spanwise measurement locations. Since the optical setup did not allow vertical translation of the laser beam, the CRM was rolled by ±3° to obtain velocity profiles above and below the wing at each spanwise position. The 24 measured profiles were combined to a two-dimensional representation of the mean streamwise velocity (freestream velocity 285.9 m/s) **(a)**. The location of the area covered by the FLEET measurements in relation to the aircraft body is shown in **(b)**.
Source: Reprinted with permission from Springer Nature, [116]. © 2021.

the displacement of the tagged region at a later instant in time with an intensified camera. Sample single-pulse FLEET images at different heights above the jet are depicted in Fig. 13. The same authors provided evidence that the FLEET signal in oxygen containing flows is almost one order of magnitude lower compared to pure nitrogen flows in [117]. Subsequently, temperature measurements were performed in heated nitrogen and air jets by spectrally resolving the FLEET emission, indicating the potential of the method for combined temperature/velocity measurements [118]. By using stereoscopic observation and operating the intensified cameras in burst mode, the measurement of 3C flow velocity, three-dimensional flow traces as well as acceleration was achieved [119]. Further development efforts of the method targeted the complex dependencies of the fluorescence signal with respect to thermodynamic conditions as well as gas composition [120–124]. In investigating the FLEET technique's uncertainty limits under thermodynamic conditions relevant to cryogenic wind tunnel testing, accuracy of the measured velocities was found to be of the order of 1% with a precision of 0.4 m/s [123]. In this study, the femtosecond laser was operated at 1 kHz repetition rate and the FLEET signal was captured at 200 kHz with a lens-coupled image intensifier/high-speed camera combination. To reach beyond the limitations imposed by the Ti:Sapphire femtosecond laser technology (low pulse energy and repetition rate limited to 10 kHz) used for FLEET tagging, the available measurement rate and pulse energy were further increased by introducing either picosecond [125–127] or femtosecond [128] burst-mode laser technology, to write the tag lines. Recently, the FLEET technique was applied at the cryogenic National Transonic Facility (NTF), NASA Langley Research Center, where it was used to identify a velocity deficit region in the wake of a Common Research Model (CRM) wing (Fig. 14) [116]. A recently published review article by Danehy et al. provides a conclusive summary on the fundamentals, past applications and future lines of development of the FLEET technique [129].

Molecular scattering techniques

In contrast to resonant LIF techniques, where the excitation frequency of the laser has to coincide with a populated electronic energy level of the probed molecule, the non-resonant scattering of light from molecules is a process that can occur at any wavelength. The incident photon excites the molecule into a virtual state, which immediately relaxes by emitting a photon, so that no lifetime can be associated with this interaction. The molecular scattering of light is further classified into two subcategories. If the wavelength of the excitation and the scattered photon coincide, the "elastic" scattering process is termed Rayleigh scattering. If there is a net energy transfer from the excitation photon to the molecule, "inelastic" spontaneous Raman scattering occurs, producing a red- (Stokes) and blue-shifted (anti-Stokes) scattering response [98,112].

Due to the technique's capability to measure the concentration of major gas species as well as temperature, laser based spontaneous Raman scattering has extensively been used for pointwise or one-dimensional flame studies [130]. Static pressure or velocity measurements are in principle possible, but have not yet been carried out. Raman scattering is about three orders of magnitude weaker compared to (already weak) Rayleigh scattering, it has no demonstrated ability to measure the pertinent flow quantities and is susceptible to strong laser stray light from walls or windows. Therefore, the technique is not discussed further in the current framework of inlet flow distortion measurement. For a single-component gas (air can be treated as such), the laser-induced Rayleigh scattering radiating from a probed volume is proportional to the gas density. Temperature or pressure can then be deduced by applying the ideal gas law, provided, that the one or the other is known. Due to the relative strength of the signal, the laser induced Rayleigh scattering can be used for planar measurements in combination with powerful lasers and sensitive detectors. However, the main difficulty to apply the technique to technical flows is posed by Mie scattering from large particles, which are commonly present in such environments, and laser stray light from surfaces like viewing windows or flow channel walls. Both occur at a similar wavelength and are typically many orders of magnitude stronger compared to molecular Rayleigh scattering. Additional flow information can be extracted from the Rayleigh signal when it is spectrally resolved: The amplitude of the spectrum is related to density, width and shape are associated with pressure and temperature and flow velocity is proportional to a Doppler shift of the entire spectrum to higher or lower frequencies [112,131]. Some point-wise measurement approaches such as CRBS (Coherent Rayleigh–Brillouin Scattering) [132–134] or IRS (Interferometric Rayleigh Scattering) [135–138] exist, which exploit the spectral properties of the scattered signal to measure multiple flow quantities simultaneously, but all suffer from the aforementioned omnipresent laser stray light in enclosed flow environments. In addition, these point-wise techniques lack sufficient spatial detail to analyse and understand complex flow topologies. Due to its stray light suppression capabilities the FRS (Filtered Rayleigh Scattering) technique is the only Rayleigh scattering approach that has the potential to compete under the demanding conditions of inlet flow distortion measurement.

FRS. The FRS method relies on the spectral discrimination between i) weak elastic laser light scattering from gas molecules inside a probe volume, which carries information on density, pressure, temperature and flow velocity (the latter through the optical Doppler frequency-shift) and ii) intense laser stray light from surfaces or large particles (Mie scattering) by means of molecular absorption. The basic principle of the method is indicated in Fig. 15. The scattered light from surfaces or particles has the same narrow bandwidth as the illuminating light

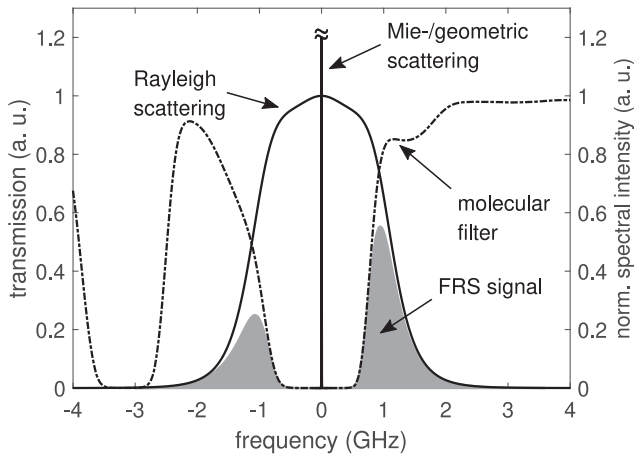

Fig. 15. Narrow bandwidth laser light scattering (Mie/geometric) is attenuated by the molecular filter (dashed–dotted), while portions of the spectrally broadened Rayleigh scattering pass through and form the FRS signal.

source, while light scattered from gas molecules is spectrally broadened. The broadening is mainly caused by the stochastic molecular (Brownian) motion. In utilising a molecular absorption line as a notch filter, narrow bandwidth laser stray light can be strongly attenuated, while portions of the Rayleigh scattered light pass through the filter and constitute the FRS signal.

By adopting the general principle of molecular filtering originally developed for LIDAR[2] applications [139], Miles and Lempert introduced the FRS technique for aerodynamic diagnostics in 1990 [140]. Miles research group and others have used the FRS technique for applications ranging from planar flow visualisation in high speed aerodynamic flows [141–145], to temperature field measurements in combustion flows [146–152]. Other work involves the combined application of PIV and FRS to measure flow and temperature field simultaneously [153,154]. Furthermore, a frequency scanning FRS method was introduced, which allows the simultaneous derivation of time-averaged pressure, temperature and velocity information [96,155–157]. However, application of the FRS technique has generally been limited to unconfined flows, i.e. to laboratory experiments, where the probed volume of interest was not inside some apparatus and therefore the laser light illumination and scattered light collection did not occur through windows. The main reason for this limitation was constituted by the intense laser light scattered from windows and walls being insufficiently attenuated by the molecular filter. This insufficient attenuation resulted from laser-line broadening effects and frequency impurities, both of which are associated with the type of pulsed laser light sources used in the past (typically injection seeded Nd: YAG lasers) [149,151,155,158–163].

Motivated by the fact that the deficient spectral purity of the formerly used pulsed laser light sources constitutes the major obstacle in exploiting the FRS method's full potential, the Engine Measurement Systems group at DLR (German Aerospace Center) Cologne developed an alternative approach to the FRS technique: In focusing on time-averaged measurements rather than instantaneous results, the system was established around a continuous wave laser. In combining a compact and robust design with superior spectral characteristics, this step forward formed the basis of opening the technique to a wide field of applications, ranging from precision laboratory experiments to turbomachinery component testing under realistic operating conditions. In adopting the aforementioned frequency scanning approach, the system has the capability to simultaneously measure time-averaged pressure, temperature and velocity fields in gaseous flows with absolute uncertainties as low as 15 hPa, 2.5 K and 2.7 m/s, respectively [164]. The modified system hardware, as well as the novel theoretical considerations, enabled the characterisation of an internal flow phenomenon by means of the FRS technique, for the first time in the literature [165]. Therein, the modified technique was used to measure pressure, temperature and flow velocity inside a circular duct using endoscopic image acquisition. By adopting the idea of observing the measurement plane from multiple views to acquire three-component velocities originally introduced for DGV [166], an FRS velocimetry system was developed [131]. In utilising multiple-branch imaging fibre technology and thus observing the measurement plane from three different sides, the simultaneous acquisition of planar pressure and temperature distributions, as well as three-component velocity fields in the near-field and far-field of a turbulent air jet was achieved (Fig. 16, for far field results see original paper). The CW laser approach was subsequently adapted by Boyda and Lowe, who extended the evaluation procedure by a cross-correlation method [167].

Apart from the FRS method's further development in the fields of theory and measurement accuracy, the novel FRS implementation was used for fundamental flow investigations in canonical laboratory flows as well as at large scale experimental facilities related to turbomachinery component testing. Regarding the former, the FRS technique was employed to gather detailed temporally averaged planar information on the temperature and velocity fields inside a Ranque–Hilsch vortex tube [169]. Observed flow structures suggested a strong coupling between acoustic phenomena and the time-averaged flow field. In addition, FRS was applied to investigate the aero-thermal flow behind the nozzle guide vane (NGV) cascade of a three-sector gas turbine combustor simulator (Fig. 17) [168]. A direct comparison of non-intrusive FRS results with data measured by a conventional five-hole probe revealed a significant bias to velocities measured by the probe, which can be attributed to strong pressure gradients present in the NGV airfoils' wake areas. Finally, the FRS technique was used to characterise the aero-thermal properties at the outlet of a high-pressure single sector combustor, operated under engine representative conditions [170,171]. In this work, a fully probe-based FRS implementation was presented, which relied on the transport of high-power laser light through optical fibres and observation with a flexible imaging fibre borescope. Results were found to be in good agreement with complementary velocity measurements by PIV and OH-LIF thermometry. Whereas OH-LIF is restricted to temperatures above 1300 K [172], FRS is capable of resolving the whole temperature range from low temperatures near the air-cooled liner walls to high temperatures at the combustor's centreline.

Ability for seeding-free distortion measurement

The previous sections provide an overview on the few laser-optical techniques with the potential to execute non-intrusive seeding-free air flow measurements. In the context of inlet flow distortion measurement in a complex experimental facility, O_2 LIF has to be considered inappropriate. The method is the least mature, relies on complex hardware and the signal-to-noise ratio is very low even under controlled laboratory conditions. CO_2 LIF based on IR laser radiation might offer an interesting alternative, since time-resolved measurements of static pressure are feasible and lineshape scanning via CW laser excitation can be used for time-averaged multi-parameter measurements. However, the technique is still in an early stage of development and further fundamental research is needed to assess the capabilities of the method. Moreover, the measurement of flow velocity using LIF is only possible along the direction of incidence of the laser, which requires two laser sheets with different directions of propagation to resolve the two in-plane velocity components. The out-of-plane component remains inaccessible to the method [96]. The development of the FLEET technique has kept progressing over the past decade, resulting in an accurate instrument for measuring flow velocity in challenging environments at acquisition

[2] Light Detection And Ranging.

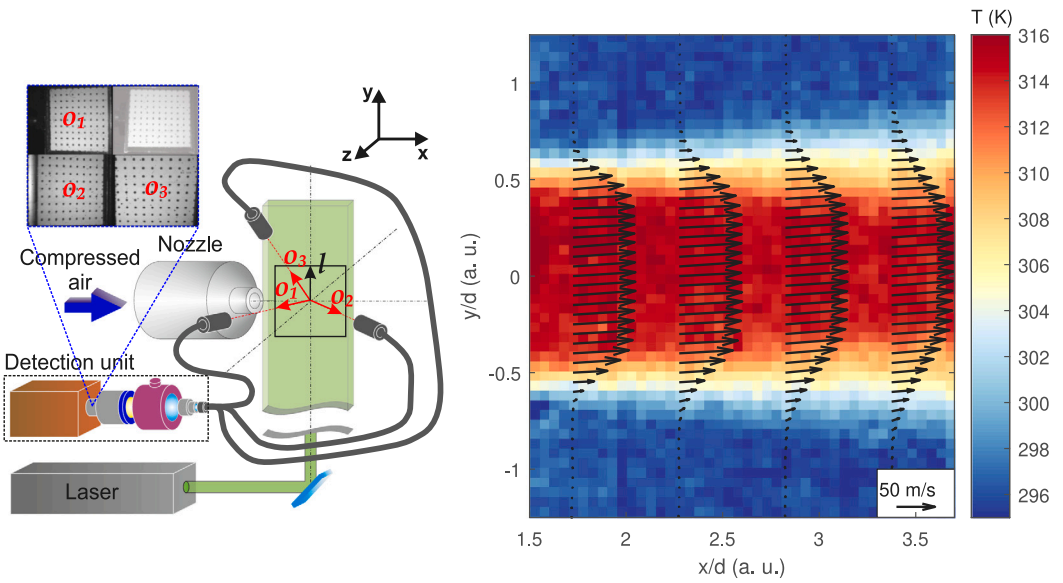

Fig. 16. (Left) Near-field characterisation of a turbulent jet: Light scattered from the interrogation area is collected from three directions by means of a multiple-branch image fibre bundle and transmitted through the detection unit, which is composed of two lenses in retro-arrangement (grey), the molecular iodine filter (pink) as well as a bandpass filter (blue). Quadrants of the resulting image represent the differing camera views. (Right) Near-field jet topology measured by FRS: Temperature and velocity fields both exhibit constant values inside the potential core near the jet axis, enveloped by strong gradients in the shear layer and ambient conditions in the surroundings.
Source: Reprinted and adapted with permission from [131].

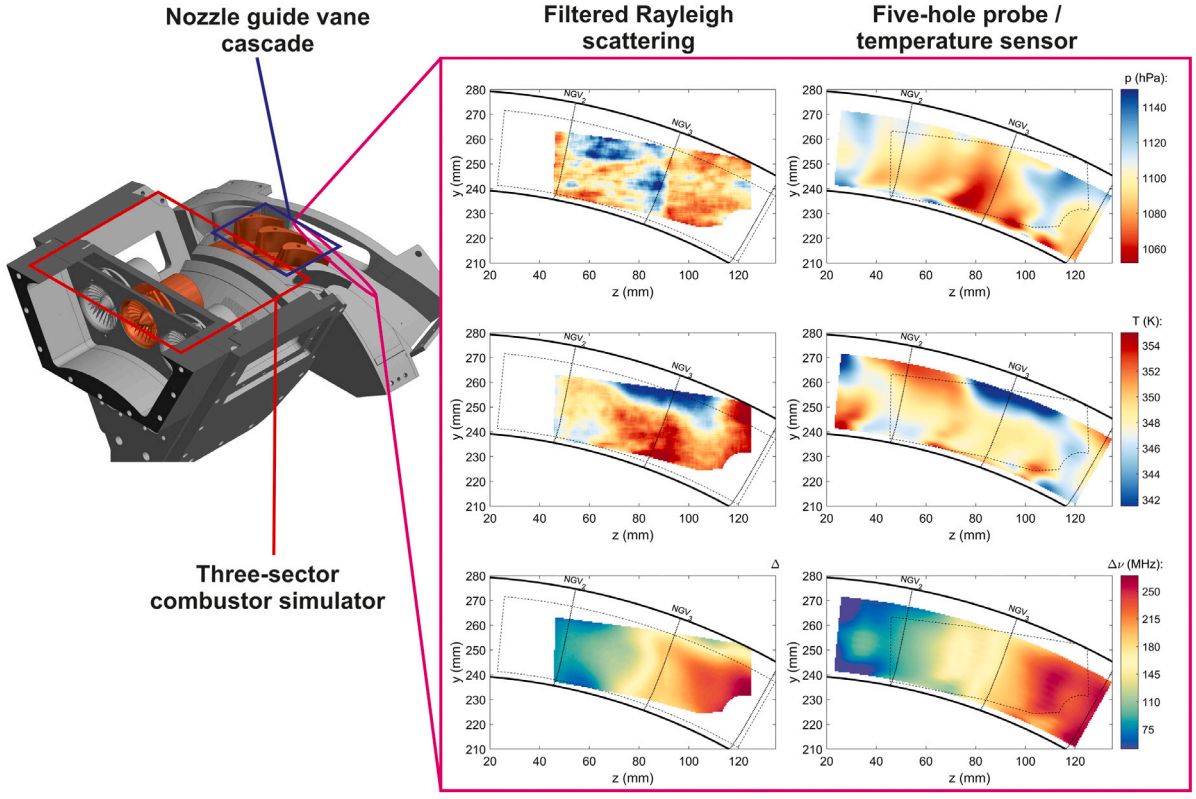

Fig. 17. A sectional view of the test rig's CAD model is shown on the left. Pre-heated air enters the three-sector lean-burn combustor simulator through the swirler elements from the left and as a result relevant temperature distortions together with a high degree of swirl (±50°) and turbulence intensity (up to ~30%) approach the NGV cascade. The investigations focus on the central sector which is coloured in orange. Measurements behind the NGV cascade were performed using a conventional five-hole probe with mounted temperature sensor and FRS. The data analysis revealed pronounced differences between the velocity results obtained by both methods, which, when combined with a CFD solution, could be attributed to erroneous probe readings due to strong pressure gradients in the wake zones of the NGV airfoils.
Source: Reprinted with permission from Springer Nature, [168]. © 2018.

rates of up to 1 MHz. However, the high fluence required to dissociate nitrogen molecules at the measurement location, can only be achieved 0-D, 1-D along a line of ~1 cm length or quasi-2-D by using multiple lines. To spatially resolve the 3C velocity distribution at the AIP would

Table 3
Summary of seeding-free optical techniques for inlet flow distortion measurement. Specified quantities are static pressure (p), flow velocity (v), static temperature (T), density (ρ), concentration (c). Simultaneous measurement of two or more quantities is denoted by "/" (e.g. $p/v/T$), time-averaged by TA, time-resolved by TR.

Technique	Measured quantities	Current state of maturity	Potential for inlet flow distortion measurement
O_2 LIF	*To date:* Visualisation *Potential:* T (TR), ρ (TR)	• Single-shot • Simple laboratory flows, mostly flames • No quantitative measurements to date • No spatial resolution/uncertainty data available	NO • Complex hardware (deep UV laser, intensified cameras) • Very weak signal
CO_2 LIF	*To date:* p (TA), T (TA), p/c (TA) *Potential:* p (TR), T (TR), $p/T/v/c$ (TR)	Simple laboratory flows • Pulsed: TA p or T, large interrogation area • CW: multi-parameter with lineshape scan at 330 fps (0.5 Hz) • No spatial resolution/uncertainty data available	Pulsed: YES • Detection limit too high for natural air • Quantitative TR not yet shown CW: YES • Further fundamental investigations needed • Laser-sheet too small
FLEET	*To date:* 3C-v (TR), T (TR) *Potential:* 3C-v/T (TR)	• 0-D, 1-D (1 cm), quasi 2D with multiple taglines • Spatial resolution: 1 mm transverse, 2–3.3 mm streamwise [123] • v with high accuracy (1%) and precision (0.4 m/s) [123] • Up to 1 MHz repetition rate • Applied to complex flows (cryogenic wind tunnel)	YES • Interrogation area too small for TR flow topology • Signal quenching by oxygen
FRS	*To date:* v (TR), T (TR), p/3C-v/T (TA) *Potential:* p (TR), 3C-v (TR), p/3C-v/T (TR)	• Planar technique, typical light sheet height 20–150 mm • Spatial resolution 0.2 mm [154] • TR measurements in simple flows only (accuracy 3–10% for single shot T) • TA $p/v/T$ in complex flows (accuracy: 50–90 hPa/2-3 K/2–3 m/s [168]), TA p/3C-v/T in simple flow (accuracy: 5 hPa/1.2 K/1.4 m/s [131])	YES • p accuracy in complex flow to be improved • TA p/3C-v/T in complex flow not yet demonstrated • Multi-parameter TR not yet demonstrated

require a stereo camera setup as well as traversing of the laser through the plane of interest, which is very time consuming and technically demanding. Furthermore, due to the small interrogation area, FLEET cannot be used to resolve the instantaneous flow topology. The FRS technique has shown its potential to measure time-resolved planar distributions of a single flow quantity (predominantly temperature) in simple flow configurations such as free flames or jets. By using a CW laser with excellent spectral characteristics, the FRS method can be used to simultaneously measure time-averaged pressure, one velocity component and temperature fields in complex internal flows. The simultaneous measurement of time-averaged thermodynamic quantities and 3C velocity field was achieved in a free jet experiment. Even though the time-resolved measurement of multiple flow variables still needs to be demonstrated, the FRS method clearly shows the highest potential to characterise inlet flow distortions in a complex experimental installation. Unlike seeding based PIV or DGV velocimetry methods used so far, the FRS technique is not limited to swirl distortion measurement but has the unique capability to simultaneously capture velocity and scalar fields and, thus, to resolve total pressure and temperature distortions. The characteristics of the different methods and their development potential for inlet flow distortion measurement are summarised in Table 3.

3.3. FRS for in-situ laser-optical distortion measurement in ground and in-flight testing

In its time-averaged variant using CW laser illumination, the seeding-free FRS technique has an immediate high potential to be used for the characterisation of intake flow distortion in complex experimental scenarios. Since the FRS method is closely related to DGV in terms of hardware requirements, the DGV approach presented in Fig. 11 serves as an excellent blueprint for applying FRS in similar configurations. To unlock the unsteady measurement potential of FRS to simultaneously measure instantaneous velocity field and scalar flow quantities, however, progress in instrumentation and novel data acquisition and evaluation strategies will be required.

Compared to DGV signals from particle scattering, the available scattered intensity by FRS is several orders of magnitude weaker. To achieve the necessary time resolution and signal-to-noise-ratio, FRS measurements at the AIP will require the usage of powerful pulsed laser light sources to capture unsteady inlet flow distortions. In this context, the aforementioned deficient spectral purity of the pulsed injection-seeded Nd:YAG laser systems used to date significantly limits the applicability of the FRS method for unsteady measurements in confined flow environments. The lack of spectral quality originates from the injection-seeded slave oscillator and is inherent for this type of laser systems [158,162]. To this end, the long pulse laser concept presented in Fig. 18[3] might prove a viable alternative. In this laser architecture, the only oscillator in the system is found inside the seed laser. Since the realisation of the required spectral properties is much simpler to achieve in these CW solid state lasers [173] and no properties of a second larger cavity have to be taken into account, the spectral purity of the system is only determined by the respective seed pulse entering the amplification stages. Thus, a significantly improved suppression of laser induced stray light is expected, which would enable the FRS technique to measure instantaneous flow data in the direct vicinity of highly luminous surfaces.

The general aim of any FRS acquisition and evaluation method is finding a solution to the multiple parameter dependency of the measured signal. One measured intensity value stands against up to five unknown flow quantities[4] (three velocity components, temperature, pressure). In addition, a minimum of three linear independent observation directions are required to unambiguously derive the three components of the velocity vector. The aforementioned frequency scanning method has successfully been used to measure multiple flow quantities simultaneously. By modulating the laser's output frequency along the molecular filter's transmission curve in discrete frequency steps, this results in intensity spectra at each camera sensor element. The number of discrete scanning frequencies is chosen to be much larger than the actual number of unknown flow quantities, which turns the evaluation into an over-determined mathematical problem. However, since an image has to be taken at each frequency step, the acquisition procedure is time consuming and cannot be applied to acquire instantaneous flow field data. To overcome these limitations,

[3] Amplitude Technologies (Continuum) Agilite laser family, https://amplitude-laser.com/products/nanosecond-lasers/nanosecond-advanced-lasers/agilite/.

[4] An equation of state is typically used to couple density and pressure/temperature.

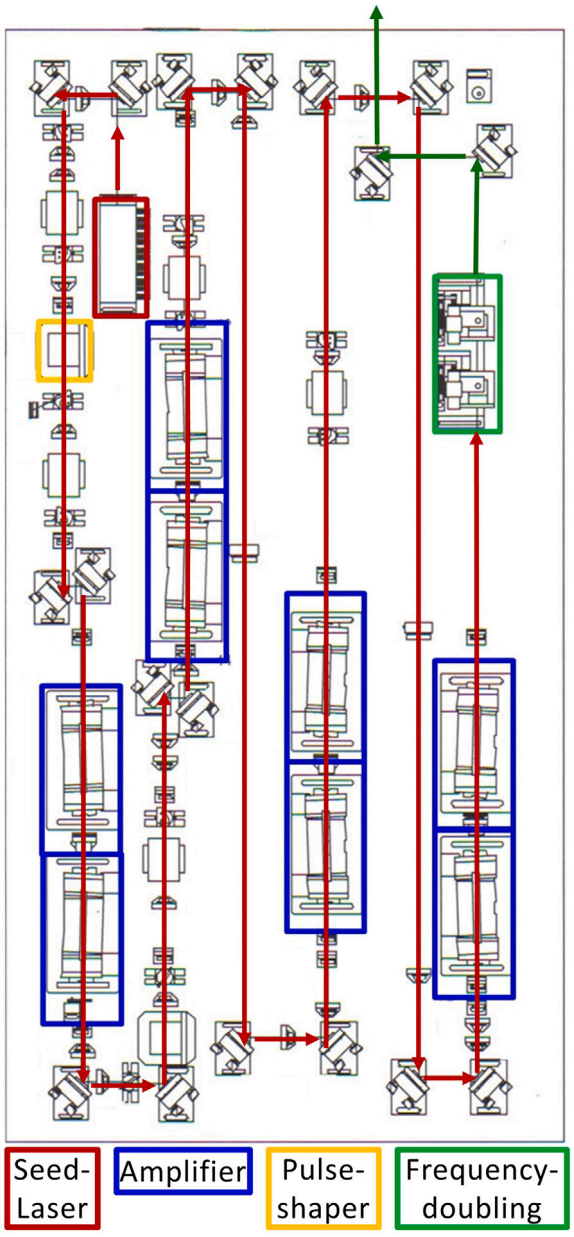

Fig. 18. Long pulse laser design: The single-longitudinal mode CW seed laser (red) is sliced and shaped into an appropriate seed pulse by an electro-optical modulator (yellow). These seed pulses are then amplified in four amplification stages (blue) and finally converted into narrow bandwidth high energy green 532 nm radiation in the second harmonic generator (green).

two imaging concepts with the potential to simultaneously acquire multiple instantaneous flow variables are depicted in Fig. 19. Both are inspired by the FRS velocimetry concept [131] and rely on multiple-branch imaging fibre technology to observe the measurement plane from multiple directions. The first configuration (Fig. 19, left) requires a minimum of five observation branches to unambiguously derive the five flow quantities of interest. The approach takes advantage of the fact that the detected intensity per resolution element is not only a function of the wanted flow quantities, but also of the scattering angle, which is defined as the inverse cosine of the scalar product of the unit vector in the laser and observer direction. The influence of the scattering angle on the signal intensity is twofold: For multiple observers, the Rayleigh scattering's spectral width and shape changes with the scattering angle, even though the thermodynamic conditions stay the same. Likewise, the detected Doppler frequency shift varies with the scattering geometry. The second approach (Fig. 19, right) uses two acquisition channels as indicated by the two cameras, each equipped with an absorption filter of differing vapour concentration (variants of this concept have been published in [174,175]). Such a configuration would require a minimum of three observation directions, which results in six independent intensity values to derive the five unknown flow quantities. In combination with pulsed laser illumination, both concepts have the capability for synchronous instantaneous 3C velocity, pressure and temperature field measurement.

The conceptual approach outlined above describes a possible pathway towards a comprehensive experimental description of both the steady and unsteady components of inlet flow distortion, using the FRS method. Further technological hurdles are introduced by an intended deployment of FRS instrumentation during flight tests. The challenges compared to ground-based measurements arise from the harsh environment (e.g. vibration, noise, altitude and relative movement of the equipment) and limitations by the aircraft platform (e.g. limited space, quality of optical access, power supply, airworthiness/certification). Furthermore, electronic equipment requiring active cooling such as lasers or scientific cameras must be placed in ambient controlled zones of the aircraft or the aircraft's operating envelope must be revised (e.g. by reduced flight altitudes) to ensure safe and reliable operation. More information on equipment specific requirements as well as certification and safety aspects in the context of advanced optical diagnostics can be drawn from the AIM (Advanced In-flight Measurement techniques) and AIM^2 project documentation and respective publications [176–178]. Previous examples of using laser-optical diagnostics in-flight are applications of point-wise LDA (Laser Doppler Anemometry) and L2F (Laser-2-Focus) techniques [179], LIDAR (Light Detection And Ranging) [180,181] and PIV [182,183] for characterising flight speeds close to the fuselage, wake vortices or overwing flow structures and turbulence. Apart from general complexities associated with the in-flight application of laser-optical flow measuring instruments regarding dimensions, weight, energy consumption and optical alignment, the reliable supply of tracer particles under flight conditions is the main challenge for techniques such as LDA, L2F or PIV [74]. Typically, the measurements have to rely on natural occurring seeding like water droplets inside clouds or particles originating from air pollution. The size distribution and concentration of these particles is highly dependent on the actual weather conditions and has significant impact on data quality and validity [179,182,183]. In view of the envisaged application scenario of measuring the flow inside extremely compact and highly integrated engine inlets, further difficulties arise from the fact that optical accessibility will be reduced to a minimum, which makes the usage of probe-based technology unavoidable. Point-wise LDA or L2F are well suited to be integrated into compact and robust probe solutions. However, these techniques lack the necessary spatial information to assess the expected complex flow patterns. In the light of these drawbacks of current in-flight measuring approaches, the seeding-free FRS method has an immediate high potential for airborne velocimetry and, in addition, has the capability to simultaneously provide static pressure and temperature [74]. In the context of optical access limitations, a fully probe-based implementation of the FRS technique with endoscopic image acquisition and high-power laser light transfer through optical fibres has already been realised [170,171]. This indicates the capabilities of the method to achieve in-situ measurements in challenging flow environments with aggravated optical accessibility requirements.

From a technological point of view, there is a high chance of successfully implementing CW FRS technology on a flying test bed to perform time-averaged in-situ flow measurements inside closely integrated engine inlet configurations. Volume, weight and electrical power consumption of such an FRS system remain moderate. The usage of fibre technology for laser light transfer and image detection allows for flexible and convenient installation through unpressurised and ambient

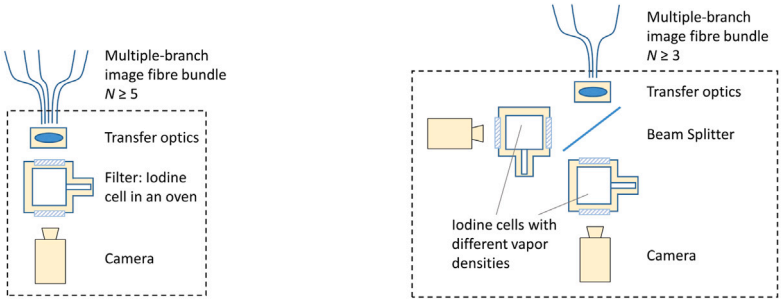

Fig. 19. Two alternative versions of FRS-camera system setups for the instantaneous measurement of 3C-velocity, temperature and pressure.

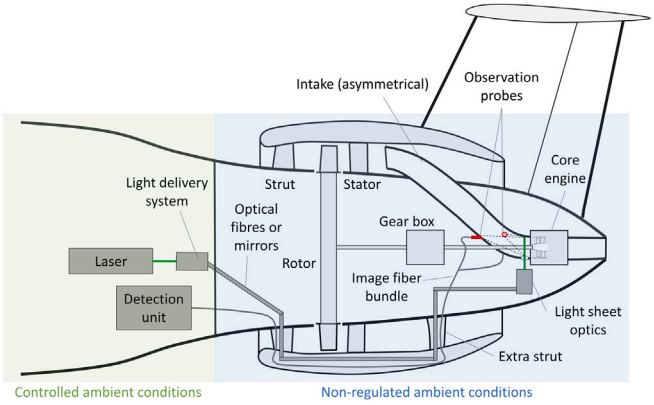

Fig. 20. Concept of an in-flight FRS measurements system installed to a closely coupled engine configuration. The integrated engine design is inspired by the Bauhaus Luftfahrt Propulsive Fuselage concept [184].

controlled zones of the aircraft. Furthermore, optical light sheet and imaging probes could be used to fully accommodate the restricted optical accessibility. In contrast, the application of pulsed laser technology to measure unsteady inlet flow distortions has certainly to be considered less mature. Apart from the significantly larger dimensions, higher weight, power and cooling requirements of such a laser system, it is questionable whether the transfer of the laser light to the test object can occur through optical fibres or whether the necessary high pulse energy (>1 J) would require an actively stabilised laser beam guidance with mirrors.

A schematic of a possible FRS in-flight implementation is provided in Fig. 20. Sensitive equipment such as the laser as well as detection unit containing the camera system and temperature stabilised iodine filter are placed inside the ambient controlled part of the aircraft. The laser beam is coupled into the light delivery system, which will preferably be based on fibre technology for both CW or pulsed laser operation. In addition to a high degree of flexibility, no optical interface between ambient controlled aircraft cabin and the non-regulated zone will be required when using fibres. If active beam guidance with mirrors is to be used for pulsed laser operation, an optical port must be designed and the controller has to account for changes in the beam path, caused by deformation of the aircraft body through thermal, pressure and g-load effects. Hollow elements of the aircraft structure can be used to deliver the laser light to the test section. Optical fibres can be installed as simple as electrical cables, while the mirror solution would require mounting brackets with remotely adjustable mirrors on the aircraft structure and additional cables for the control signal. The laser is then directed into the beam forming optics and the light sheet enters the test section through an optical access to illuminate the AIP. The collection of the FRS signal occurs through observation probes, which are flush-mounted at several positions (two are indicated in red in Fig. 20) around the flow channel. To measure all three components of flow velocity combined with static pressure and temperature, at least three camera views are required for CW and five for pulsed laser operation. Furthermore, a stronger inclination of the different views is potentially beneficial for measurement accuracy. An enlarged schematic view of such an optical probe is shown in Fig. 21. The front end of the probe consists of a collecting lens, which images the plane of interest onto the entry face of an image fibre bundle. The oblique observation results in object areas outside the front lens' specified depth of field, so that the collecting lens and image fibre bundle surface are aligned at an angle to satisfy the Scheimpflug criterion for sharp imaging of the light sheet throughout the visible domain. Since the perspective arrangement may result in areas that are obscured from observation, this has to be compensated by the additional probes. Similar to the optical fibres used for laser light transport, flexible image fibres can be guided through hollow structural elements to the ambient controlled aircraft cabin containing the detection unit.

A possible solution to relax the requirements for unsteady measurements using pulsed laser radiation, is posed by the multi-pass concept shown in Fig. 22. Instead of spanning a light sheet to illuminate the complete cross section of the inlet duct, the unconditioned laser beam enters the test section from below. After the first pass, the beam is deflected by two mirrors fixed inside a hollow shroud and directed back into the flow. This is repeated several times, so that a regular pattern of crossing laser beams fills the cross section (the arrangement shown is only to illustrate the concept, several more passes could be implemented). Except for the red transparent region, where the laser direction is undefined and detector saturation can be expected, 3C velocity, static pressure and temperature can be inferred at each resolution element along the individual beam traces. If a sufficient angular resolution is realised from a large number of passes, two-dimensional maps can be generated by interpolation. Such a setup would be beneficial in a number of ways: (1) By illuminating the cross section with a laser beam pattern instead of spanning the full width with a light sheet, more than two orders of magnitude less laser energy is required to reach similar FRS signal levels. (2) Since significantly reduced laser energy needs to be introduced into the test section, this notably increases the chance of transmitting the laser light by means of optical waveguides for pulsed laser operation. Earlier work on fibre optic beam delivery for PIV measurements showed that pulse energies of 30 mJ can be transmitted [185]. (3) No installation of beam forming optics is required at the test section. This not only eliminates a potential source of error, but also significantly reduces the optical access requirements for laser illumination to a small bore instead of a large window.

As far as the future prospects of such in-flight measuring systems are concerned, it can be anticipated that their development will significantly improve the current state-of-the-art in several aspects. Firstly, in-flight measurements could be used for engine stability assessment in line with the established stability metrics to determine the sensitivity of the propulsion system to the intake distortion, especially for transient in-flight operating conditions, which are not possible to be reproduced in ground tests. Secondly, the assessment of the unsteady

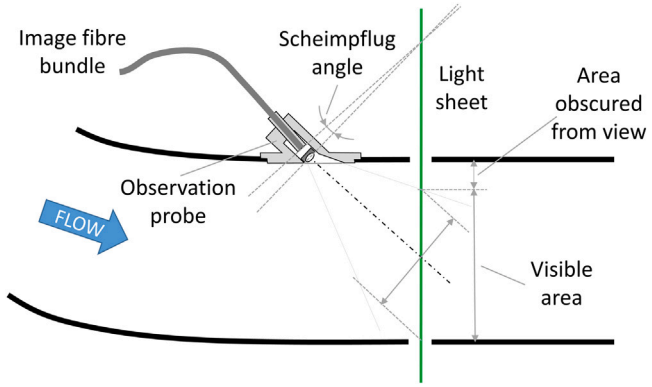

Fig. 21. Possible layout of a fibre-optical imaging probe and optical arrangement.

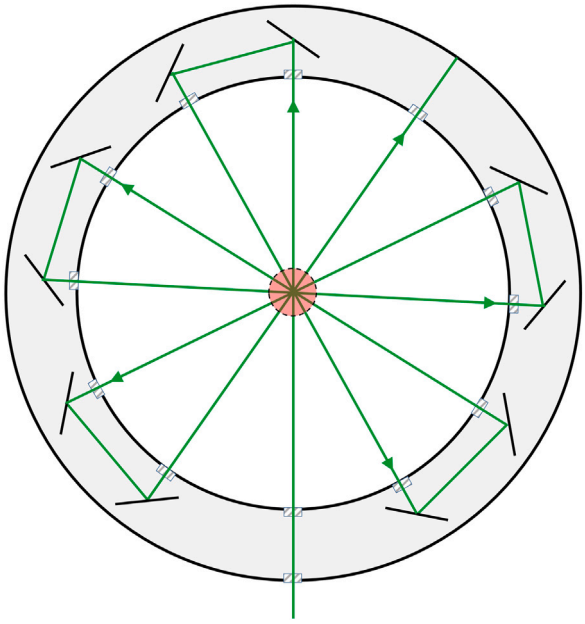

Fig. 22. Concept of a multi-pass arrangement: The laser beam enters from below and is deflected multiple times into the test section. The red area marks the intersection region, where evaluation will not be feasible due to beam overlap.

swirl distortion could aid in the determination of the aeromechanical compatibility between intake and rotor blades. New methods have been recently developed to assess the flow distortion approaching rotating blades [50]. The evaluation of the unsteady incidence signature on the blades can give insights on the blade loading distribution. This can be linked with the formation of stall cells [186] and, thus, can be correlated with the engine stability. Finally, the FRS technique will offer additional capabilities to simultaneously measure velocity and scalar fields, so that data required to derive all established metrics could be obtained with a single, seeding-free, non-intrusive instrument. Moreover, the potential to simultaneously measure unsteady velocity, pressure and temperature by FRS opens the path for the development of completely new distortion metrics based on scalar-velocity correlations.

4. Conclusion

Novel airframe designs, with integrated engine architectures, offer potential benefits in terms of an increased aircraft efficiency and noise reduction. However, a major risk arises from inlet flow distortion caused by BLI and convoluted engine intakes, such that the possible gain in aerodynamic efficiency might be partially offset by the effect of the distorted propulsor inflow on fan performance. To unlock the full potential of these novel concepts, a close integration of airframe and engine design and development is imperative.

Historically, inlet distortion has been treated as a steady state event and several descriptors have been developed in academics and industry. Despite efforts to develop standardised metrics by the S-16 committee of SAE International, no unique set of distortion descriptors has been established to date. Multi-hole or total pressure probe rakes are typically used for time-averaged measurement of the relevant quantities to derive total pressure and swirl distortion metrics. However, the steady state picture utterly neglects the dynamic component of inlet flow distortion, which can reach magnitudes of up to 30% of the time-averaged quantities. Furthermore, the combination of different types of distortions is an underdeveloped field and there is a great lack of understanding of the impact that these events can have on the stability budget of an engine. To capture the unsteady dimension of the problem, the state-of-the-art for measuring total pressure distortion relies on miniature high-speed pressure transducers mounted on rake arrays, rotor blades or in blade passages, at acquisition rates on the order of 10 kHz. However, since the method is intrusive, a balance has to be found between the unavoidable flow channel blockage and spatial resolution necessary to capture the relevant flow details. Efforts to characterise swirl distortion at the AIP employing non-intrusive laser-optical DGV and stereoscopic PIV, increased the number of available datapoints by orders of magnitude. But the provision of appropriate seeding poses a major difficulty of these methods, which motivated the review on seeding-free laser-optical measurement techniques. In this context, the FRS technique is found to have the highest potential for characterising inlet flow distortions, since the method has the proven ability to simultaneously measure velocity, static pressure and temperature fields in complex experimental installations. Moreover, a fully probe-based realisation of FRS has already been implemented, underpinning the unique ability to use FRS technology along the entire engine development cycle in ground and in-flight testing.

Even though non-intrusive diagnostics has been successfully introduced in the framework of inlet flow distortion measurement, there is an urgent need to develop novel measuring and analytical methods to meet the anticipated demand for more comprehensive flow information, due to the effects of highly convoluted intake architectures. To this end, this article identifies FRS measurement technology as a promising candidate, but further development efforts in suitable laser light sources, acquisition and evaluation procedures is needed to open the technique to unsteady inlet flow distortion measurement. The modification of established steady-state distortion descriptors to incorporate previously unavailable unsteady flow data and the development of novel distortion metrics, is currently an area of active research and will continue to gain importance as future developments of aircraft with fuselage-integrated engine concepts progress. This alignment of capability is setting the stage for exciting research questions and provides opportunities for close collaboration of academia and industry, to foster faster and more educated design choices, ultimately leading to shorter innovation cycles and reduced time-to-market of next-generation aircraft designs.

Declaration of competing interest

The authors declare that they have no known competing financial interests or personal relationships that could have appeared to influence the work reported in this paper.

Acknowledgements

The SINATRA project leading to this publication has received funding from the Clean Sky 2 Joint Undertaking (JU) under grant agreement No 886521. The JU receives support from the European Union's Horizon 2020 research and innovation programme and the Clean Sky 2 JU members other than the Union.

References

[1] NASA Stragetic Implementation Plan - 2019 Update, Tech. rep, National Aeronautics and Space Administration (NASA), 2019, URL https://www.nasa.gov/sites/default/files/atoms/files/sip-2019-v7-web.pdf.

[2] Strategic Research and Innovation Agenda - 2017 Update, Tech. rep, Advisory Council for Aviation Research and Innovation in Europe (ACARE), 2017, URL https://www.acare4europe.org/sites/acare4europe.org/files/document/ACARE-Strategic-Research-Innovation-Volume-1.pdf.

[3] European commission – directorate general for research and innovation & directorate general for mobility and transport, in: Flightpath 2050: Europe's vision for aviation, The Publications Office of the European Union, Luxembourg, 2011, http://dx.doi.org/10.2777/50266.

[4] C.A. Hall, D. Crichton, Engine and installation configurations for a silent aircraft, in: XVII International Symposium on Air Breathing Engines, ISABE, American Institute of Aeronautics and Astronautics, Munich, Germany, 2005.

[5] H. Kim, M.-S. Liou, Flow simulation of N2B hybrid wing body configuration, in: 50th AIAA Aerospace Sciences Meeting Including the New Horizons Forum and Aerospace Exposition, American Institute of Aeronautics and Astronautics, Nashville, USA, 2012, http://dx.doi.org/10.2514/6.2012-838.

[6] J.R. Lucas, W.F. O'Brien, A.M. Ferrar, Effect of BLI–type inlet distortion on turbofan engine performance, in: ASME Turbo Expo: Turbine Technical Conference and Exposition, American Society of Mechanical Engineers, Düsseldorf, Germany, 2014, http://dx.doi.org/10.1115/GT2014-26666.

[7] A. Castillo Pardo, C.A. Hall, Aerodynamics of boundary layer ingesting fuselage fans, J. Turbomach. 143 (4) (2021) 041007, http://dx.doi.org/10.1115/1.4049918.

[8] A. Seitz, A.s.L. Habermann, F. Peter, F. Troeltsch, A. Castillo Pardo, B. Della Corte, M. van Sluis, Z. Goraj, M. Kowalski, X. Zhao, T. Grönstedt, J. Bijewitz, G. Wortmann, Proof of concept study for fuselage boundary layer ingesting propulsion, Aerospace 8 (1) (2021) http://dx.doi.org/10.3390/aerospace8010016.

[9] J. Welstead, J.L. Felder, Conceptual design of a single-aisle turboelectric commercial transport with fuselage boundary layer ingestion, in: 54th AIAA Aerospace Sciences Meeting, American Institute of Aeronautics and Astronautics, San Diego, USA, 2016, http://dx.doi.org/10.2514/6.2016-1027.

[10] R.P. Rademakers, R. Niehuis, S. Bindl, Influence of secondary flow within integrated engine inlets on the performance and stability of a jet engine, in: XXII International Symposium on Air Breathing Engines, ISABE, Phoenix, USA, 2015, URL http://hdl.handle.net/2374.UC/745645.

[11] M.M. Wojewodka, C. White, K. Kontis, A review of flow control techniques and optimisation in S-shaped ducts, Int. J. Heat Fluid Flow (2017) 48, http://dx.doi.org/10.1016/j.ijheatfluidflow.2018.06.016.

[12] M. Drela, Development of the D8 transport configuration, in: 29th AIAA Applied Aerodynamics Conference, American Institute of Aeronautics and Astronautics, Honolulu, Hawaii, 2011, http://dx.doi.org/10.2514/6.2011-3970.

[13] E.M. Greitzer, H.N. Slater, N+3 Aircraft Concept Designs and Trade Studies, Final Report, Tech. rep, National Aeronautics and Space Administration (NASA), 2010, p. 183.

[14] A. Uranga, M. Drela, E.M. Greitzer, D.K. Hall, N.A. Titchener, M.K. Lieu, N.M. Siu, C. Casses, A.C. Huang, G.M. Gatlin, J.A. Hannon, Boundary layer ingestion benefit of the D8 transport aircraft, AIAA J. 55 (11) (2017) 3693–3708, http://dx.doi.org/10.2514/1.J055755.

[15] L. Wiart, O. Atinault, B. Paluch, D. Hue, R. Grenon, Development of NOVA aircraft configurations for large engine integration studies, in: 33rd AIAA Applied Aerodynamics Conference, American Institute of Aeronautics and Astronautics, Dallas, USA, 2015, http://dx.doi.org/10.2514/6.2015-2254.

[16] H.D. Kim, J.L. Felder, M. Armstrong, Revolutionary aeropropulsion concept for sustainable aviation: Turboelectric distributed propulsion, in: XXI International Symposium on Air Breathing Engines, ISABE, Busan, Korea, 2013, URL https://core.ac.uk/display/42733509.

[17] E. de la Rosa Blanco, C. Hall, D. Crichton, Challenges in the silent aircraft engine design, in: 45th AIAA Aerospace Sciences Meeting and Exhibit, American Institute of Aeronautics and Astronautics, Reno, USA, 2007, http://dx.doi.org/10.2514/6.2007-454.

[18] G. McLelland, D.G. MacManus, P.K. Zachos, D. Gil-Prieto, M. Migliorini, Influence of upstream total pressure profiles on S-duct intake flow distortion, J. Propul. Power 36 (3) (2020) 346–356, http://dx.doi.org/10.2514/1.B37554.

[19] W.T. Cousins, History, philosophy, physics, and future directions of aircraft propulsion system/inlet integration, in: ASME Turbo Expo: Turbine Technical Conference nd Exposition, Vol.2, American Society of Mechanical Engineers, Vienna, Austria, 2004, http://dx.doi.org/10.1115/GT2004-54210.

[20] S-16 Turbine Engine Inlet Flow Distortion Committee, Inlet Total-Pressure-Distortion Considerations for Gas-Turbine Engines, AIR1419C, Tech. rep, SAE International, 2017, p. 226, http://dx.doi.org/10.4271/AIR1419C.

[21] S-16 Turbine Engine Inlet Flow Distortion Committee, Assessment of the Inlet/Engine Total Temperature Distortion Problem, AIR5867, Tech. rep, SAE International, 2017, p. 57, http://dx.doi.org/10.4271/AIR5867.

[22] S-16 Turbine Engine Inlet Flow Distortion Committee, A Methodology for Assessing Inlet Swirl Distortion, AIR5686, Tech. rep, SAE International, 2017, p. 110, http://dx.doi.org/10.4271/AIR5686.

[23] S-16 Turbine Engine Inlet Flow Distortion Committee, Guidelines for Characterization of Gas Turbine Engine Total-Pressure, Planar-Wave, and Total-Temperature Inlet-Flow Distortion, ARP6420, Tech. rep, SAE International, 2021, p. 34, http://dx.doi.org/10.4271/ARP6420.

[24] Sutrisno, T.A. Rohmat, S.B. Wibowo, S. Iswahyudi, Vortex dynamics study of the canard deflection angles' influence on the Sukhoi Su-30-like model to improve stall delays at high AoA, Aerosp. 6 (2) (2019) 12, http://dx.doi.org/10.3390/aerospace6020012.

[25] A. Dowling, T. Hynes, Towards a silent aircraft, Aeronaut. J. 110 (1110) (2006) 487–494, http://dx.doi.org/10.1017/S000192400000138X.

[26] A. Coschignano, H. Babinsky, Boundary-layer development downstream of normal shock in transonic intakes at incidence, AIAA J. 57 (12) (2019) 5241–5251, http://dx.doi.org/10.2514/1.J058508.

[27] S-16 Turbine Engine Inlet Flow Distortion Committee, Gas Turbine Engine Inlet Flow Distortion Guidelines, ARP1420C, Tech. rep, SAE International, 2017, p. 25, http://dx.doi.org/10.4271/ARP1420C.

[28] C. Reid, The response of axial flow compressors to intake flow distortion, in: ASME 1969 Gas Turbine Conference and Products Show, American Society of Mechanical Engineers, Cleveland, USA, 1969, http://dx.doi.org/10.1115/69-GT-29.

[29] A.F. Campbell, An Investigation of Distortion Indices for Prediction of Stalling Behavior in Aircraft Gas Turbine Engines, (Ph.D. thesis), Virginia Polytechnic Institute and State University, 1981, URL https://vtechworks.lib.vt.edu/bitstream/handle/10919/95571/LD5655.V855_1981.C343.pdf?sequence=1.

[30] E.M. Greitzer, Review–axial compressor stall phenomena, J. Fluids Eng. 102 (2) (1980) 134–151, http://dx.doi.org/10.1115/1.3240634.

[31] K.-S. Song, S.-G. Kim, Y.-H. Hwang, Failure of the J79 engine compressor blade due to stall, J. Fail. Anal. Prev. 7 (3) (2007) 212–217, http://dx.doi.org/10.1007/s11668-007-9034-4.

[32] J. Melick, H. C., Analysis of inlet flow distortion and turbulence effects on compressor stability, Tech. rep, NASA CR-114577, LTV Aerospace Corp.; Vought Systems Div.;, Dallas, TX, US, 1973, p. 215, URL https://ntrs.nasa.gov/search.jsp?R=19730012966.

[33] W. Cousins, A theory for the prediction of compressor blade aerodynamic response, in: 34th AIAA/ASME/SAE/ASEE Joint Propulsion Conference and Exhibit, in: Joint Propulsion Conferences, American Institute of Aeronautics and Astronautics, Cleveland,USA, 1998, http://dx.doi.org/10.2514/6.1998-3308.

[34] J.P. Longley, H.W. Shin, R.E. Plumley, P.D. Silkowski, I.J. Day, E.M. Greitzer, C.S. Tan, D.C. Wisler, Effects of rotating inlet distortion on multistage compressor stability, J. Turbomach. 118 (2) (1996) 181–188, http://dx.doi.org/10.1115/1.2836624.

[35] B. Brimelow, T. Collins, G. Pfefferkorn, Engine testing in a dynamic environment, in: 10th Propulsion Conference, American Institute of Aeronautics and Astronautics, San Diego, CA, USA, 1974, http://dx.doi.org/10.2514/6.1974-1198.

[36] R.J. Wenzel, L. M.; Blaha, Analysis of Dynamic Inlet Distortion Applied to a Parallel Compressor Model, Tech. rep, NASA-TM-X-3522,NASA Technical Memorandum TM-X-3522, NASA Lewis Research Center;, Cleveland, OH, US, 1977, p. 25, URL https://ntrs.nasa.gov/search.jsp?R=19770015161.

[37] P.D. Silkowski, Measurements of Rotor Stalling in a Matched and a Mismatched Multistage Compressor, Tech. rep, GTL-221GTL, Gas Turbine Laboratory, Massachusetts Institute of Technology, Cambridge, MA, 1995, URL http://hdl.handle.net/1721.1/1047644.

[38] C. Freeman, A.L. Rowe, Intake engine interactions of a modern large turbofan engine, in: ASME 1999 International Gas Turbine and Aeroengine Congress and Exhibition, American Society of Mechanical Engineers, Indianapolis, IN, USA, 1999, http://dx.doi.org/10.1115/99-GT-344.

[39] T. Breuer, N.C. Bissinger, Basic principles - gas turbine compatibility - gas turbine aspects, in: Encyclopedia of Aerospace Engineering, John Wiley & Sons, Ltd, Chichester, UK, 2010, http://dx.doi.org/10.1002/9780470686652.eae573, arXiv:arXiv:1011.1669v3.

[40] C. Tan, I. Day, S. Morris, A. Wadia, Spike-type compressor stall inception, detection, and control, Annu. Rev. Fluid Mech. 42 (1) (2010) 275–300, http://dx.doi.org/10.1146/annurev-fluid-121108-145603.

[41] M. Shaw, An Assessment of CFD for Transonic Fan Stabilities Studies, (Ph.D. thesis), Queens' College, University of Cambridge, 2015.

[42] T. Dejene Toge, A.M. Pradeep, Experimental investigation of stall inception and its propagation in a contra rotating axial fan under radial inflow distortion, in: ASME Turbo Expo: Turbine Technical Conference and Exposition, American Society of Mechanical Engineers, Charlotte, North Carolina, USA, 2017, http://dx.doi.org/10.1115/GT2017-63432.

[43] A.J. Provenza, K.P. Duffy, M.A. Bakhle, Aeromechanical response of a distortion-tolerant boundary layer ingesting fan, J. Eng. Gas Turbines Power 141 (1) (2019) http://dx.doi.org/10.1115/1.4040739.

[44] W. Zhang, M. Vahdati, A parametric study of the effects of inlet distortion on fan aerodynamic stability, J. Turbomach. 141 (1) (2019) http://dx.doi.org/10.1115/1.4041376.

[45] Y. Liu, E. Stumpf, Estimation of vehicle-level fuel burn benefits of aircraft formation flight, J. Aircraft 55 (2) (2018) 853–861, http://dx.doi.org/10.2514/1.C034296.

[46] Airbus and its partners demonstrate how sharing the skies can save airlines fuel and reduce CO2 emissions, Tech. rep, Airbus Press Release, 2021.

[47] G.A. Richardson, W.N. Dawes, A.M. Savill, An unsteady, moving mesh CFD simulation for Harrier hot-gas ingestion control analysis, Aeronaut. J. 111 (1117) (2007) 133–144, http://dx.doi.org/10.1017/S0001924000004395.

[48] T.J. Biesiadny, W.M. Braithwaite, R.H. Soeder, M. Abdelwahab, Summary of Investigations of Engine Response to Distorted Inlet Conditions, Tech. rep, NASA TM-87317, Lewis Research Center, Cliveland, Ohio, 1986, p. 215, URL https://ntrs.nasa.gov/citations/19860016864.

[49] S.R. Wellborn, B.A. Reichert, T.H. Okiishi, Study of the compressible flow in a diffusing S-duct, J. Propuls. Power 10 (5) (1994) 668–675, http://dx.doi.org/10.2514/3.23778.

[50] M. Migliorini, P.K. Zachos, D.G. MacManus, Novel method for evaluating intake unsteady flow distortion, J. Propuls. Power 38 (1) (2021) 135–147, http://dx.doi.org/10.2514/1.B38127.

[51] J.P. Murphy, D.G. MacManus, Ground vortex aerodynamics under crosswind conditions, Exp. Fluids 50 (1) (2011) 109–124, http://dx.doi.org/10.1007/s00348-010-0902-4.

[52] Ç. Atalayer, J. Friedrichs, D. Wulff, Aerodynamic investigation of S-duct intake for high power turboprop installed on a channel wing, Aeronaut. J. 121 (1242) (2017) 1131–1146, http://dx.doi.org/10.1017/aer.2017.46.

[53] B. Bouldin, Y. Sheoran, Inlet flow angularity descriptors proposed for use with gas turbine engines, in: World Aviation Congress & Exposition, SAE International, Phoenix, USA, 2002, http://dx.doi.org/10.4271/2002-01-2919.

[54] F. Aulehla, Intake swirl - a major disturbance parameter in engine/intake compatibility, in: 13th Congress of ICAS/AIAA, MBB-FE124-S-PUB–74, Seattle, WA, US, 1982, URL http://hdl.handle.net/10068/164048.

[55] A. Hamed, K. Numbers, Inlet distortion considerations for high cycle fatigue in gas turbine engine, in: AIAA/ASME/SAE/ASEE 33rd Joint Propulsion Conference and Exhibit, American Institute of Aeronautics and Astronautics, Seattle, WA, US, 1997, http://dx.doi.org/10.2514/6.1997-3364.

[56] M. Lecht, H. Weyer, On the unsteady aerodynamic rotor blade loading in a transonic axial flow compressor with unsteady-state inlet distortion, in: IUTAM Symposium on Aeroelasticity in Turbomachines, Paris, France, 1976, pp. 1–16.

[57] M. Lecht, H. Weyer, Unsteady Rotor Blade Loading in an Axial Compressor with Steady-state Inlet Distortions, Tech. rep, AGARD CP 248-30, AGARD CP 248-30, Cleveland, OH, US, 1978.

[58] G.A. Mitchell, Effect of Inlet Ingestion of a Wing Tip Vortex on Compressor Face Flow and Turbojet Stall Margin, Tech. rep, NASA-TM-X-3246, E-8213,NASA Technical Memorandum TM-X-3246, Washington D.C., US, 1975, p. 78, URL https://ntrs.nasa.gov/search.jsp?R=19750018896.

[59] A. Mehdi, Effect of Swirl Distortion on Gas Turbine Operability, (Ph.D. thesis), Propulsion Engineering Centre, School of Aerospace, Transport and Manufacturing, Cranfield University, 2014.

[60] A. Naseri, M. Boroomand, S. Sammak, Numerical investigation of effect of inlet swirl and total-pressure distortion on performance and stability of an axial transonic compressor, J. Therm. Sci. 25 (6) (2016) 501–510, http://dx.doi.org/10.1007/s11630-016-0891-6.

[61] B. Tu, L. Zhang, J. Hu, Effect of swirl on the performance and stability of transonic axial compressor, Proc. Inst. Mech. Eng., Part A 232 (6) (2018) 608–621, http://dx.doi.org/10.1177/0957650917742320.

[62] J. Jacocks, Statistical analysis of distortion factors, in: AIAA 1972-1100, 8th Joint Propulsion Specialist Conference, November 1972, 1972, http://dx.doi.org/10.2514/6.1972-1100.

[63] M. Davis, A. Hale, D. Beale, An argument for enhancement of the current inlet distortion ground test practice for aircraft gas turbine engines, J. Turbomach. 124 (2) (2002) 235–241, http://dx.doi.org/10.1115/1.1451087.

[64] T. Williams, C. Hall, M. Wilson, Low pressure ratio transonic fan stall with radial distortion, J. Glob. Power Propuls. Soc. 4 (2020) 226–237, http://dx.doi.org/10.33737/jgpps/130478.

[65] D. Kidman, J. Brownlow, B. Binkley, C. Morris, Application of extreme value statistics to reduce test and computational requirements for quantifying engine inlet total pressure distortion, in: Presentation for OA Forum DoD, Academia and Industry Statistics Workshop, 2016.

[66] S-16 Turbine Engine Inlet Flow Distortion Committee, An Assessment of Planar Waves, AIR5866A, Tech. rep, SAE International, 2021, p. 64, http://dx.doi.org/10.4271/AIR5866A.

[67] Y. Sheoran, B. Bouldin, R. Hoover, M. Matwey, A centrifugal compressor operability correlation with combined total pressure and swirl distortion, in: Volume 1: Aircraft Engine; Fans and Blowers; Marine; Honors and Awards, American Society of Mechanical Engineers, Charlotte, North Carolina, USA, 2017, http://dx.doi.org/10.1115/GT2017-63721.

[68] W.M. Braithwaite, R.H. Soeder, Combined pressure and temperature distortion effects on internal flow of a turbofan engine, J. Aircraft 17 (7) (1980) 468–472, http://dx.doi.org/10.2514/3.57927.

[69] G. Tanguy, D.G. MacManus, E. Garnier, P.G. Martin, Characteristics of unsteady total pressure distortion for a complex aero-engine intake duct, Aerosp. Sci. Technol. 78 (2018) 297–311, http://dx.doi.org/10.1016/j.ast.2018.04.031.

[70] D. Gil-Prieto, D.G. MacManus, P.K. Zachos, A. Bautista, Assessment methods for unsteady flow distortion in aero-engine intakes, Aerosp. Sci. Technol. 72 (2018) 292–304, http://dx.doi.org/10.1016/j.ast.2017.10.029.

[71] D. Gil-Prieto, P.K. Zachos, D.G. MacManus, G. McLelland, Unsteady characteristics of S-duct intake flow distortion, Aerosp. Sci. Technol. 84 (2019) 938–952, http://dx.doi.org/10.1016/j.ast.2018.10.020.

[72] S-16 Turbine Engine Inlet Flow Distortion Committee, Inlet/Engine Compatibility - From Model to Full Scale Development, AIR5687A, Tech. rep, SAE International, 2016, http://dx.doi.org/10.4271/air5687a.

[73] P.K. Zachos, D.G. MacManus, D.G. Prieto, N. Chiereghin, Flow distortion measurements in convoluted aeroengine intakes, AIAA J. 54 (9) (2016) 2819–2832, http://dx.doi.org/10.2514/1.J054904, Publisher: American Institute of Aeronautics and Astronautics.

[74] K.T. Lowe, Laser velocimetry for turbofan inlet distortion applications, Aircr. Eng. Aerosp. Tec. 92 (1) (2020) 20–26, http://dx.doi.org/10.1108/AEAT-11-2018-0285, publisher: Emerald Publishing Limited.

[75] M. Raffel, C.E. Willert, F. Scarano, C.J. Kähler, S.T. Wereley, J. Kompenhans, Particle Image Velocimetry, Springer International Publishing, 2018, http://dx.doi.org/10.1007/978-3-319-68852-7.

[76] K.M. Hoopes, A New Method for Generating Swirl Inlet Distortion for Jet Engine Research, (Master thesis), Virginia Tech, 2013, URL https://vtechworks.lib.vt.edu/handle/10919/49545.

[77] T. Guimaraes Bucalo, K.T. Lowe, W.F. O'Brien, An overview of recent results using the StreamVane method for generating tailored swirl distortion in jet engine research, in: 54th AIAA Aerospace Sciences Meeting, in: AIAA SciTech Forum, American Institute of Aeronautics and Astronautics, San Diego, USA, 2016, http://dx.doi.org/10.2514/6.2016-0534.

[78] M. Nelson, K.T. Lowe, W.F. O'Brien, K.M. Hoopes, Stereoscopic PIV measurements of swirl distortion on a full-scale turbofan engine inlet, in: 52nd Aerospace Sciences Meeting, in: AIAA SciTech Forum, American Institute of Aeronautics and Astronautics, National Harbor, USA, 2014, http://dx.doi.org/10.2514/6.2014-0533.

[79] T. Guimarães, K.T. Lowe, W.F. O'Brien, Streamvane turbofan inlet swirl distortion generator: Mean flow and turbulence structure, J. Propuls. Power 34 (2) (2018) 340–353, http://dx.doi.org/10.2514/1.B36422, Publisher: American Institute of Aeronautics and Astronautics.

[80] T. Guimarães, K. Todd Lowe, W.F. O'Brien, Complex flow generation and development in a full-scale turbofan inlet, J. Eng. Gas Turbines Power 140 (8) (2018) http://dx.doi.org/10.1115/1.4039179.

[81] T. Guimarães, K.T. Lowe, W.F. O'Brien, Particle image velocimetry for distorted turbofan engine inlet applications, in: 19th International Symposium on the Application of Laser and Imaging Techniques To Fluid Mechanics, Lisbon, Portugal, 2018.

[82] J.F. Meyers, H. Komine, Doppler global velocimetry-a new way to look at velocity, in: ASME Fourth International Conference on Laser Anemometry, Cleveland, USA, 1991.

[83] H. Komine, System for measuring velocity field of fluid flow utilizing a laser-doppler spectral image converter, (US4919536A) 1990, URL https://patents.google.com/patent/US4919536/en.

[84] I. Roehle, Laser-Doppler-Velocimetry auf der Basis frequenzselektiver Absorption: Aufbau und Einsatz eines Doppler Global Velocimeters, (Ph.D. thesis), Ruhr Universität Bochum, Bochum, 1999.

[85] I. Roehle, Three-dimensional Doppler global velocimetry in the flow of a fuel spray nozzle and in the wake region of a car, Flow Meas. Instrum. 7 (3) (1996) 287–294, http://dx.doi.org/10.1016/S0955-5986(97)00011-3.

[86] C. Willert, G. Stockhausen, J. Klinner, C. Lempereur, P. Barricau, P. Loiret, J.C. Raynal, Performance and accuracy investigations of two Doppler global velocimetry systems applied in parallel, Meas. Sci. Technol. 18 (8) (2007) 2504, http://dx.doi.org/10.1088/0957-0233/18/8/027, publisher: IOP Publishing.

[87] U. Dierksheide, P. Meyer, T. Hovestadt, W. Hentschel, Endoscopic 2D particle image velocimetry (PIV) flow field measurements in IC engines, Exp. Fluids 33 (6) (2002) 794–800, http://dx.doi.org/10.1007/s00348-002-0499-3.

[88] M. Kegalj, H.-P. Schiffer, Endoscopic PIV measurements in a low pressure turbine rig, Exp. Fluids 47 (4) (2009) 689, http://dx.doi.org/10.1007/s00348-009-0712-8.

[89] D. Kim, L. Rao, H. Oh, S. Kook, Endoscopic high-speed particle image velocimetry (eHS-PIV) in a high tumble production engine, Exp. Fluids 61 (10) (2020) 219, http://dx.doi.org/10.1007/s00348-020-03055-w.

[90] R. Schlüßler, M. Bermuske, J. Czarske, A. Fischer, Simultaneous three-component velocity measurements in a swirl-stabilized flame, Exp. Fluids 56 (10) (2015) 183, http://dx.doi.org/10.1007/s00348-015-2055-y.

[91] A.J. Saltzman, K.T. Lowe, W.F. Ng, 250 kHz Three-component Doppler velocimetry at 32 simultaneous points: a new capability for high speed flows, Meas. Sci. Technol. 31 (9) (2020) 095302, http://dx.doi.org/10.1088/1361-6501/ab8ee9, Publisher: IOP Publishing.

[92] A.J. Saltzman, K.T. Lowe, W.F. Ng, 50 kHz Doppler global velocimetry for the study of large-scale turbulence in supersonic flows, Exp. Fluids 62 (9) (2021) 192, http://dx.doi.org/10.1007/s00348-021-03286-5.

[93] S.J. Thorpe, N. Quinlan, R.W. Ainsworth, The characterisation and application of a pulsed neodymium YAG laser DGV system to a time-varying high-speed flow, Opt. Laser Technol. 32 (7) (2000) 543–555, http://dx.doi.org/10.1016/S0030-3992(00)00096-7.

[94] M.A.F. Kendall, N.J. Quinlan, S.J. Thorpe, R.W. Ainsworth, B.J. Bellhouse, Measurements of the gas and particle flow within a converging-diverging nozzle for high speed powdered vaccine and drug delivery, Exp. Fluids 37 (1) (2004) 128–136, http://dx.doi.org/10.1007/s00348-004-0792-4.

[95] R.L. McKenzie, M.S. Reinath, Three dimensional planar Doppler velocity measurements in a full-scale rotor wake, AIAA J. 43 (3) (2005) 489–499, http://dx.doi.org/10.2514/1.12205.

[96] J.N. Forkey, Development and demonstration of filtered Rayleigh scattering: a laser based flow diagnostic for planar measurement of velocity, temperature, and pressure, (Ph.D. thesis), Princeton University, 1996.

[97] J.N. Forkey, W.R. Lempert, R.B. Miles, Observation of a 100-MHz frequency variation across the output of a frequency-doubled injection-seeded unstable-resonator Q-switched nd:YAG laser, Opt. Lett. 22 (4) (1997) 230–232, http://dx.doi.org/10.1364/OL.22.000230.

[98] C. Tropea, A.L. Yarin, J.F. Foss, Springer Handbook of Experimental Fluid Mechanics, in: Springer handbooks, Springer, Berlin, 2007, http://dx.doi.org/10.1007/978-3-540-30299-5.

[99] R.K. Hanson, R.M. Spearrin, C.S. Goldenstein, Spectroscopy and Optical Diagnostics for Gases, Springer International Publishing, Cham, 2016, http://dx.doi.org/10.1007/978-3-319-23252-2.

[100] G. Massey, C. Lemon, Feasibility of measuring temperature and density fluctuations in air using laser-induced O2 fluorescence, event: IEEE J. Quantum Electron. 20 (5) (1984) 454–457, http://dx.doi.org/10.1109/JQE.1984.1072427.

[101] P. Andresen, A. Bath, W. Gröger, H.W. Lülf, G. Meijer, J.J. ter Meulen, Laser-induced fluorescence with tunable excimer lasers as a possible method for instantaneous temperature field measurements at high pressures: checks with an atmospheric flame, Appl. Opt. 27 (2) (1988) 365–378, http://dx.doi.org/10.1364/AO.27.000365.

[102] R.B. Miles and, W.R. Lempert, Quantitative flow visualization in unseeded flows, Annu. Rev. Fluid Mech. 29 (1) (1997) 285–326, http://dx.doi.org/10.1146/annurev.fluid.29.1.285.

[103] R.B. Miles, J.J. Connors, P.J. Howard, E.C. Markovitz, G.J. Roth, Proposed single-pulse two-dimensional temperature and density measurements of oxygen and air, Opt. Lett. 13 (3) (1988) 195–197, http://dx.doi.org/10.1364/OL.13.000195, publisher: Optical Society of America.

[104] G. Laufer, R.L. McKenzie, D.G. Fletcher, Method for measuring temperatures and densities in hypersonic wind tunnel air flows using laser-induced O2 fluorescence, Appl. Opt. 29 (33) (1990) 4873–4883, http://dx.doi.org/10.1364/AO.29.004873, publisher: Optical Society of America.

[105] M. Smith, W. Williams, L. Price, Applicability of dual-line LIF-O2 method for measurements in engine test facilities, in: 4th AlAA International Aerospace Planes Conference, American Institute of Aeronautics and Astronautics, Orlando, USA, 1992, http://dx.doi.org/10.2514/6.1992-5089.

[106] J. Kiefer, B. Zhou, J. Zetterberg, Z. Li, M. Alden, Laser-induced fluorescence detection of hot molecular oxygen in flames using an alexandrite laser, Appl. Spectrosc. (2014) http://dx.doi.org/10.1366/14-07512, publisher: SAGE PublicationsSage UK: London, England.

[107] M. Schultze, J. Mantzaras, F. Grygier, R. Bombach, Hetero-/homogeneous combustion of syngas mixtures over platinum at fuel-rich stoichiometries and pressures up to 14bar, Proc. Combust. Inst. 35 (2) (2015) 2223–2231, http://dx.doi.org/10.1016/j.proci.2014.05.018.

[108] B.J. Kirby, R.K. Hanson, Linear excitation schemes for IR planar-induced fluorescence imaging of CO and CO_2, Appl. Opt. 41 (6) (2002) 1190–1201, http://dx.doi.org/10.1364/AO.41.001190, publisher: Optical Society of America.

[109] B.J. Kirby, R.K. Hanson, CO2 imaging with saturated planar laser-induced vibrational fluorescence, Appl. Opt. 40 (33) (2001) 6136–6144, http://dx.doi.org/10.1364/AO.40.006136, publisher: Optical Society of America.

[110] D.A. Rothamer, R.K. Hanson, Temperature and pressure imaging using infrared planar laser-induced fluorescence, Appl. Opt. 49 (33) (2010) 6436–6447, http://dx.doi.org/10.1364/AO.49.006436, publisher: Optical Society of America.

[111] C.S. Goldenstein, V.A. Miller, R.K. Hanson, Infrared planar laser-induced fluorescence with a CW quantum-cascade laser for spatially resolved CO2 and gas properties, Appl. Phys. B 120 (2) (2015) 185–199, http://dx.doi.org/10.1007/s00340-015-6167-0.

[112] P.M. Danehy, B.F. Bathel, C.T. Johansen, M. Winter, S. O'Byrne, A.D. Cutler, Molecular-Based Optical Diagnostics for Hypersonic Nonequilibrium Flows, American Institute of Aeronautics and Astronautics, Reston, VA, 2015, http://dx.doi.org/10.2514/4.103292.

[113] D.G. Bohl, M.M. Koochesfahani, B.J. Olson, Development of stereoscopic molecular tagging velocimetry, Exp. Fluids 30 (3) (2001) 302–308, http://dx.doi.org/10.1007/s003480000178.

[114] R.B. Miles, J.J. Connors, E.C. Markovitz, P.J. Howard, G.J. Roth, Instantaneous profiles and turbulence statistics of supersonic free shear layers by Raman excitation plus laser-induced electronic fluorescence (relief) velocity tagging of oxygen, Exp. Fluids 8 (1) (1989) 17–24, http://dx.doi.org/10.1007/BF00203060.

[115] J.B. Michael, M.R. Edwards, A. Dogariu, R.B. Miles, Femtosecond laser electronic excitation tagging for quantitative velocity imaging in air, Appl. Opt. 50 (26) (2011) 5158–5162, http://dx.doi.org/10.1364/AO.50.005158, publisher: Optical Society of America.

[116] D.T. Reese, R.J. Thompson, R.A. Burns, P.M. Danehy, Application of femtosecond-laser tagging for unseeded velocimetry in a large-scale transonic cryogenic wind tunnel, Exp. Fluids 62 (5) (2021) 99, http://dx.doi.org/10.1007/s00348-021-03191-x.

[117] J. Michael, M. Edwards, A. Dogariu, R. Miles, Velocimetry by femtosecond laser electronic excitation tagging (FLEET) of air and nitrogen, in: 50th AIAA Aerospace Sciences Meeting Including the New Horizons Forum and Aerospace Exposition, American Institute of Aeronautics and Astronautics, Nashville, USA, 2012, http://dx.doi.org/10.2514/6.2012-1053.

[118] M.R. Edwards, A. Dogariu, R.B. Miles, Simultaneous temperature and velocity measurements in air with femtosecond laser tagging, AIAA J. 53 (8) (2015) 2280–2288, http://dx.doi.org/10.2514/1.J053685.

[119] P.M. Danehy, B.F. Bathel, N.D. Calvert, A. Dogariu, R.B. Miles, Three component velocity and acceleration measurement using FLEET, in: 30th AIAA Aerodynamic Measurement Technology and Ground Testing Conference, in: AIAA AVIATION Forum, American Institute of Aeronautics and Astronautics, Atlanta, USA, 2014, http://dx.doi.org/10.2514/6.2014-2228.

[120] N.J. DeLuca, R.B. Miles, W.D. Kulatilaka, N. Jiang, J.R. Gord, Femtosecond laser electronic excitation tagging (FLEET) fundamental pulse energy and spectral response, in: 30th AIAA Aerodynamic Measurement Technology and Ground Testing Conference, American Institute of Aeronautics and Astronautics, Atlanta, USA, 2014, http://dx.doi.org/10.2514/6.2014-2227.

[121] N. Calvert, Y. Zhang, R.B. Miles, Characterizing FLEET for aerodynamic measurements in various gas mixtures and non-air environments, in: 32nd AIAA Aerodynamic Measurement Technology and Ground Testing Conference, American Institute of Aeronautics and Astronautics, Washington, D.C., USA, 2016, http://dx.doi.org/10.2514/6.2016-3206.

[122] Y. Zhang, R.B. Miles, Femtosecond laser tagging for velocimetry in argon and nitrogen gas mixtures, Opt. Lett. 43 (3) (2018) 551–554, http://dx.doi.org/10.1364/OL.43.000551, publisher: Optical Society of America.

[123] R.A. Burns, C.J. Peters, P.M. Danehy, Unseeded velocimetry in nitrogen for high-pressure, cryogenic wind tunnels: part I. Femtosecond-laser tagging, Meas. Sci. Technol. 29 (11) (2018) 115302, http://dx.doi.org/10.1088/1361-6501/aade1b, publisher: IOP Publishing.

[124] C.J. Peters, R.A. Burns, R.B. Miles, P.M. Danehy, Effect of low temperatures and pressures on signal, lifetime, accuracy and precision of femtosecond laser tagging velocimetry, Meas. Sci. Technol. (2020) http://dx.doi.org/10.1088/1361-6501/abc577.

[125] N. Jiang, J.G. Mance, M.N. Slipchenko, J.J. Felver, H.U. Stauffer, T. Yi, P.M. Danehy, S. Roy, Seedless velocimetry at 100 khz with picosecond-laser electronic-excitation tagging, Opt. Lett. 42 (2) (2017) 239–242, http://dx.doi.org/10.1364/OL.42.000239, publisher: Optical Society of America.

[126] R.A. Burns, P.M. Danehy, N. Jiang, M.N. Slipchenko, J. Felver, S. Roy, Unseeded velocimetry in nitrogen for high-pressure cryogenic wind tunnels: part II. Picosecond-laser tagging, Meas. Sci. Technol. 29 (11) (2018) 115203, http://dx.doi.org/10.1088/1361-6501/aade15, publisher: IOP Publishing.

[127] Z. Zhang, N. Jiang, M.N. Slipchenko, J.G. Mance, S. Roy, Picosecond laser electronic excitation tagging velocimetry using a picosecond burst-mode laser, Appl. Opt. AO60 (15) (2021) C60–C67, http://dx.doi.org/10.1364/AO.419491.

[128] J.M. Fisher, M.E. Smyser, M.N. Slipchenko, S. Roy, T.R. Meyer, Burst-mode femtosecond laser electronic excitation tagging for khz–MHz seedless velocimetry, Opt. Lett. 45 (2) (2020) 335–338, http://dx.doi.org/10.1364/OL.380109, publisher: Optical Society of America.

[129] P.M. Danehy, R.A. Burns, D.T. Reese, J.E. Retter, S.P. Kearney, FLEET velocimetry for aerodynamics, Annu. Rev. Fluid Mech. 54 (1) (2022) 525–553, http://dx.doi.org/10.1146/annurev-fluid-032321-025544.

[130] A. Ehn, J. Zhu, X. Li, J. Kiefer, Advanced laser-based techniques for gas-phase diagnostics in combustion and aerospace engineering, Appl. Spectrosc. 71 (3) (2017) 341–366, http://dx.doi.org/10.1177/0003702817690161.

[131] U. Doll, G. Stockhausen, C. Willert, Pressure, temperature, and three-component velocity fields by filtered Rayleigh scattering velocimetry, Opt. Lett. 42 (19) (2017) 3773–3776, http://dx.doi.org/10.1364/OL.42.003773.

[132] X. Pan, M.N. Shneider, R.B. Miles, Coherent Rayleigh-Brillouin scattering, Phys. Rev. Lett. 89 (18) (2002) 183001, http://dx.doi.org/10.1103/PhysRevLett.89.183001.

[133] X. Pan, P.F. Barker, A. Meschanov, J.H. Grinstead, M.N. Shneider, R.B. Miles, Temperature measurements by coherent Rayleigh scattering, Opt. Lett. 27 (3) (2002) 161, http://dx.doi.org/10.1364/OL.27.000161.

[134] A. Gerakis, M.N. Shneider, Towards single shot gas flow velocity and temperature measurements with coherent Rayleigh-Brillouin scattering, in: AIAA Scitech 2019 Forum, American Institute of Aeronautics and Astronautics, San Diego, USA, 2019, http://dx.doi.org/10.2514/6.2019-1326.

[135] R.G. Seasholtz, A.E. Buggele, M.F. Reeder, Flow measurements based on Rayleigh scattering and Fabry-Perot interferometer, Opt. Laser Eng. 27 (6) (1997) 543–570, http://dx.doi.org/10.1016/S0143-8166(96)00063-2.

[136] A.F. Mielke, R.G. Seasholtz, K.A. Elam, J. Panda, Time-average measurement of velocity, density, temperature, and turbulence velocity fluctuations using Rayleigh and Mie scattering, Exp. Fluids 39 (2) (2005) 441–454, http://dx.doi.org/10.1007/s00348-005-0990-8.

[137] J. Panda, Spectrally-resolved Rayleigh scattering to measure velocity, temperature, density, and density fluctuations in high-speed flows, Exp. Fluids 61 (3) (2020) 74, http://dx.doi.org/10.1007/s00348-020-2903-2.

[138] A.D. Cutler, K. Rein, S. Roy, P.M. Danehy, N. Jiang, 100-Khz interferometric Rayleigh scattering for multi-parameter flow measurements, Opt. Express 28 (3) (2020) 3025–3040, http://dx.doi.org/10.1364/OE.380934, publisher: Optical Society of America.

[139] H. Shimizu, S.A. Lee, C. She, High spectral resolution lidar system with atomic blocking filters for measuring atmospheric parameters, Appl. Opt. 22 (9) (1983) 1373–1381, http://dx.doi.org/10.1364/AO.22.001373.

[140] R. Miles, W. Lempert, Two-dimensional measurement of density, velocity, and temperature in turbulent high-speed air flows by UV Rayleigh scattering, Appl. Phys. B: Photophys. Laser Chem. 51 (1) (1990) 1–7, http://dx.doi.org/10.1007/BF00332317.

[141] R. Miles, W. Lempert, J. Forkey, Instantaneous velocity fields and background suppression by filtered Rayleigh scattering, in: 29th Aerospace Sciences Meeting, American Institute of Aeronautics and Astronautics, Reno, USA, 1991, http://dx.doi.org/10.2514/6.1991-357.

[142] R. Miles, J. Forkey, W. Lempert, Filtered Rayleigh scattering measurements in supersonic/hypersonic facilities, in: 28th Joint Propulsion Conference and Exhibit, American Institute of Aeronautics and Astronautics, Nashville, USA, 1992, http://dx.doi.org/10.2514/6.1992-3894.

[143] J. Forkey, S. Cogne, A. Smits, S. Bogdonoff, W. Lempert, R. Miles, Time-sequenced and spectrally filtered Rayleigh imaging of shock wave and boundary layer structure for inlet characterization, in: 29th Joint Propulsion Conference and Exhibit, American Institute of Aeronautics and Astronautics, Monterey, USA, 1993, http://dx.doi.org/10.2514/6.1993-2300.

[144] R. Miles, W. Lempert, J. Forkey, N. Finkelstein, P. Erbland, Quantifying high speed air flows by light scattering from air molecules, in: Fluid Dynamics Conference, American Institute of Aeronautics and Astronautics, Colorado Springs, USA, 1994, http://dx.doi.org/10.2514/6.1994-2230.

[145] J. Forkey, W. Lempert, S. Bogdonoff, R. Miles, G. Russell, Volumetric imaging of supersonic boundary layers using filtered Rayleigh scattering background suppression, in: 32nd Aerospace Sciences Meeting and Exhibit, American Institute of Aeronautics and Astronautics, Reno, USA, 1994, http://dx.doi.org/10.2514/6.1994-491.

[146] G.S. Elliott, N. Glumac, C.D. Carter, A.S. Nejad, Two-dimensional temperature field measurements using a molecular filter based technique, Combust. Sci. Technol. 125 (1–6) (1997) 351–369, http://dx.doi.org/10.1080/00102209708935663.

[147] D. Hoffman, K.-U. Münch, A. Leipertz, Two-dimensional temperature determination in sooting flames by filtered Rayleigh scattering, Opt. Lett. 21 (7) (1996) 525, http://dx.doi.org/10.1364/OL.21.000525.

[148] D. Most, A. Leipertz, Simultaneous two-dimensional flow velocity and gas temperature measurements by use of a combined particle image velocimetry and filtered Rayleigh scattering technique, Appl. Opt. 40 (30) (2001) 5379, http://dx.doi.org/10.1364/AO.40.005379.

[149] S.P. Kearney, R.W. Schefer, S.J. Beresh, T.W. Grasser, Temperature imaging in nonpremixed flames by joint filtered Rayleigh and Raman scattering, Appl. Opt. 44 (9) (2005) 1548, http://dx.doi.org/10.1364/AO.44.001548.

[150] J. Zetterberg, Z. Li, M. Afzelius, M. Aldén, Two-dimensional temperature measurements in flames using filtered Rayleigh scattering at 254 nm, Appl. Spectrosc. 62 (7) (2008) 778–783, publisher: Society for Applied Spectroscopy.

[151] D. Müller, R. Pagel, A. Burkert, V. Wagner, W. Paa, Two-dimensional temperature measurements in particle loaded technical flames by filtered Rayleigh scattering, Appl. Opt. 53 (9) (2014) 1750, http://dx.doi.org/10.1364/AO.53.001750.

[152] T.A. McManus, J.A. Sutton, Quantitative planar temperature imaging in turbulent non-premixed flames using filtered Rayleigh scattering, Appl. Opt. 58 (11) (2019) 2936, http://dx.doi.org/10.1364/AO.58.002936.

[153] D. Most, F. Dinkelacker, A. Leipertz, Direct determination of the turbulent flux by simultaneous application of filtered Rayleigh scattering thermometry and particle image velocimetry, Proc. Combust. Inst. 29 (2) (2002) 2669–2677, http://dx.doi.org/10.1016/S1540-7489(02)80325-X.

[154] T.A. McManus, J.A. Sutton, Simultaneous 2D filtered Rayleigh scattering thermometry and stereoscopic particle image velocimetry measurements in turbulent non-premixed flames, Exp. Fluids 61 (6) (2020) 134, http://dx.doi.org/10.1007/s00348-020-02973-z.

[155] J.N. Forkey, N.D. Finkelstein, W.R. Lempert, R.B. Miles, Demonstration and characterization of filtered Rayleigh scattering for planar velocity measurements, AIAA J. 34 (3) (1996) 442–448, http://dx.doi.org/10.2514/3.13087.

[156] J.N. Forkey, W.R. Lempert, R.B. Miles, Accuracy limits for planar measurements of flow field velocity, temperature and pressure using filtered Rayleigh scattering, Exp. Fluids 24 (2) (1998) 151–162, http://dx.doi.org/10.1007/s003480050162.

[157] M. Boguszko, G.S. Elliott, On the use of filtered Rayleigh scattering for measurements in compressible flows and thermal fields, Exp. Fluids 38 (1) (2005) 33–49, http://dx.doi.org/10.1007/s00348-004-0881-4.

[158] R.G. Seasholtz, A.E. Buggele, Improvement in suppression of pulsed nd:YAG laser light with iodine absorption cells for filtered Rayleigh scattering measurements, in: Optical Technology in Fluid, Thermal, and Combustion Flow III, Vol.3172, International Society for Optics and Photonics, 1997, pp. 625–635, http://dx.doi.org/10.1117/12.293414.

[159] P.M. Allison, T.A. McManus, J.A. Sutton, Quantitative fuel vapor/air mixing imaging in droplet/gas regions of an evaporating spray flow using filtered Rayleigh scattering, Opt. Lett. 41 (6) (2016) 1074, http://dx.doi.org/10.1364/OL.41.001074.

[160] C. Ground, L. Maddalena, Visualization of supersonic turbulent vortical flows with filtered Rayleigh scattering, J. Vis.-Jap. 20 (1) (2017) 75–86, http://dx.doi.org/10.1007/s12650-016-0382-6.

[161] Y. Krishna, A.M. Elbaz, Y. Yue, G. Magnotti, Mole fraction measurement through a transparent quarl burner using filtered Rayleigh scattering, Appl. Opt. 58 (20) (2019) 5575, http://dx.doi.org/10.1364/AO.58.005575.

[162] R.A. Patton, J.A. Sutton, Seed laser power effects on the spectral purity of Q-switched nd:YAG lasers and the implications for filtered Rayleigh scattering measurements, Appl. Phys. B 111 (3) (2013) 457–468, http://dx.doi.org/10.1007/s00340-013-5358-9.

[163] J.A. Sutton, R.A. Patton, Improvements in filtered Rayleigh scattering measurements using Fabry–Perot etalons for spectral filtering of pulsed, 532-nm nd:YAG output, Appl. Phys. B 116 (3) (2014) 681–698, http://dx.doi.org/10.1007/s00340-013-5752-3.

[164] U. Doll, E. Burow, G. Stockhausen, C. Willert, Methods to improve pressure, temperature and velocity accuracies of filtered Rayleigh scattering measurements in gaseous flows, Meas. Sci. Technol. 27 (12) (2016) 125204, http://dx.doi.org/10.1088/0957-0233/27/12/125204.

[165] U. Doll, G. Stockhausen, C. Willert, Endoscopic filtered Rayleigh scattering for the analysis of ducted gas flows, Exp. Fluids 55 (3) (2014) http://dx.doi.org/10.1007/s00348-014-1690-z.

[166] D.S. Nobes, H.D. Ford, R.P. Tatam, Instantaneous, three-component planar Doppler velocimetry using imaging fibre bundles, Exp. Fluids 36 (1) (2004) 3–10, http://dx.doi.org/10.1007/s00348-003-0586-0.

[167] M. Boyda, G. Byun, K.T. Lowe, Investigation of velocity and temperature measurement sensitivities in cross-correlation filtered Rayleigh scattering (CCFRS), Meas. Sci. Technol. 30 (4) (2019) 044004, http://dx.doi.org/10.1088/1361-6501/ab0350.

[168] U. Doll, M. Dues, T. Bacci, A. Picchi, G. Stockhausen, C. Willert, Aero-thermal flow characterization downstream of an NGV cascade by five-hole probe and filtered Rayleigh scattering measurements, Exp. Fluids 59 (10) (2018) 150, http://dx.doi.org/10.1007/s00348-018-2607-z.

[169] U. Doll, E. Burow, M. Beversdorff, G. Stockhausen, C. Willert, C. Morsbach, D. Schlüß, M. Franke, The flow field inside a Ranque-Hilsch vortex tube part I: Experimental analysis using planar filtered Rayleigh scattering, in: 9th International Symposium on Turbulence and Shear Flow Phenomena, TSFP 2015, Vol.2, Melbourne, Australia, 2015.

[170] M. Schroll, U. Doll, G. Stockhausen, U. Meier, C. Willert, C. Hassa, I. Bagchi, Flow field characterization at the outlet of a lean burn single-sector combustor by laser-optical methods, J. Eng. Gas Turbines Power 139 (1) (2017) http://dx.doi.org/10.1115/1.4034040.

[171] U. Doll, G. Stockhausen, J. Heinze, U. Meier, C. Hassa, I. Bagchi, Temperature measurements at the outlet of a lean burn single-sector combustor by laser optical methods, J. Eng. Gas Turbines Power 139 (2) (2017) http://dx.doi.org/10.1115/1.4034355.

[172] J. Heinze, U. Meier, T. Behrendt, C. Willert, K.-P. Geigle, O. Lammel, R. Lückerath, PLIF thermometry based on measurements of absolute concentrations of the OH radical, Z. Phys. Chem 225 (11–12) (2011) 1315–1341, http://dx.doi.org/10.1524/zpch.2011.0168.

[173] W. Koechner, Solid-State Laser Engineering, Vol. 1, 6, Springer, 2006, http://dx.doi.org/10.1007/0-387-29338-8.

[174] M.G. Boguszko, Measurements In Fluid Flows Using Filtered Rayleigh Scattering, (Ph.D. thesis), Rutgers, The State University of New Jersey, 2003.

[175] T.P. Jenkins, J. George, D. Feng, R.B. Miles, Filtered Rayleigh scattering for instantaneous measurements of pressure and temperature in gaseous flows, in: AIAA Scitech 2019 Forum, American Institute of Aeronautics and Astronautics, San Diego, USA, 2019, http://dx.doi.org/10.2514/6.2019-1324.

[176] Final Report Summary - AIM (Advanced in-flight measurement Techniques) | Report Summary | FP6, CORDIS | European Commission, URL https://cordis.europa.eu/project/id/30827/reporting.

[177] Final Report Summary - AIM^2 (Advanced In-flight Measurement Techniques 2) | Report Summary | FP7, CORDIS | European Commission, URL https://cordis.europa.eu/project/id/266107/reporting.

[178] F. Boden, N. Lawson, H.W. Jentink, J. Kompenhans (Eds.), Advanced in-flight measurement techniques, in: Research Topics in Aerospace, Springer Berlin Heidelberg, Berlin, Heidelberg, 2013, http://dx.doi.org/10.1007/978-3-642-34738-2.

[179] M. Beversdorff, W. Förster, R. Schodl, H.W. Jentink, In-flight laser anemometry for aerodynamic investigations on an aircraft, Opt. Laser Eng. 27 (6) (1997) 571–586, http://dx.doi.org/10.1016/S0143-8166(96)00064-4.

[180] R.K. Bogue, H.W. Jentink, Optical Air Flow Measurements in Flight, Tech. rep, National Aeronautics and Space Administration (NASA), 2004, p. 101.

[181] H.W. Jentink, R.K. Bogue, Optical air flow measurements for flight tests and flight testing optical air flow meters, Tech. rep, National Aerospace Laboratory (NLR), 2005.

[182] C. Dunker, R. Geisler, Full-scale in-flight flow investigation of a high-lift vortex system by means of particle image velocimetry, in: New Results in Numerical and Experimental Fluid Mechanics XI, in: posts on Numerical Fluid Mechanics and Multidisciplinary Design, Springer International Publishing, Cham, Germany, 2018, pp. 523–532, http://dx.doi.org/10.1007/978-3-319-64519-3_47.

[183] C. Dunker, An in-flight investigation of a turbulent boundary layer at Reynolds numbers up to Re_{ϕ}=49,400, Exp. Fluids 62 (1) (2021) 4, http://dx.doi.org/10.1007/s00348-020-03072-9.

[184] Bauhaus Luftfahrt https://www.bauhaus-luftfahrt.net/de/topthema/propulsive-fuselage/ (Accessed 16 April 2021).

[185] D.P. Hand, J.D. Entwistle, R.R.J. Maier, A. Kuhn, C.A. Greated, J.D.C. Jones, Fibre optic beam delivery system for high peak power laser PIV illumination, Meas. Sci. Technol. 10 (3) (1999) 239–245, http://dx.doi.org/10.1088/0957-0233/10/3/021.

[186] J.E. Giuliani, J.-P. Chen, Fan response to boundary-layer ingesting inlet distortions, AIAA J. 54 (10) (2016) 3232–3243, http://dx.doi.org/10.2514/1.J054762.

2022-03-09

Non-intrusive flow diagnostics for unsteady inlet flow distortion measurements in novel aircraft architectures

Doll, Ulrich

Elsevier

Doll U, Migliorini M, Baikie J, et al., (2022) Non-intrusive flow diagnostics for unsteady inlet flow distortion measurements in novel aircraft architectures, Progress in Aerospace Sciences, Volume 130, April 2022, Article number 100810

https://doi.org/10.1016/j.paerosci.2022.100810